FINNISH METEOROLOGICAL INSTITUTE
CONTRIBUTIONS

No. 36

TERRESTRIAL SUBSTORMS AS A PART OF GLOBAL ENERGY FLOW

Eija I. Tanskanen

Theoretical Physics Division
Department of Physical Sciences
Faculty of Science
University of Helsinki
Helsinki, Finland

To be presented, with the permission of the Faculty of Science of the University of Helsinki, for public criticism in the Small Auditorium E204 at Physicum in Kumpula Campus on March 19th, 2002, at 10 o'clock a.m.

Finnish Meteorological Institute
Helsinki, 2002

ISBN 951-697-558-5 (print)
ISBN 952-10-0423-1 (pdf)
ISSN 0782-6117

Yliopistopaino
Helsinki 2002

Published by Finnish Meteorological Institute
P.O. Box 503
FIN-00101 Helsinki
Finland

Name and number of publication
Contributions 36, FMI-CONT-36
Date
March 2002

Authors
Eija I. Tanskanen

Name of project

Commissioned by

Title
Terrestrial substorms as a part of global energy flow

Abstract
The aim of this thesis is to examine terrestrial substorms. The thesis consists of an introductory part and five original research papers. The introduction gives an overview of energetics and main characteristics of substorms, whereas the research papers give a more detailed description of the studies.

The solar wind consists of a huge amount of energy of which only about 1% dissipates into the magnetosphere. Magnetic substorms, occurring several times in each day, are important components carrying solar wind energy into the terrestrial magnetosphere-ionosphere system. Main energy dissipation channels are ionospheric Joule heating, auroral precipitation, the ring current and magnetotail processes, such as plasmoid release and plasma sheet heating. Statistical results of more than 800 substorms show that ionospheric dissipation, mainly the Joule heating, covers more than half of the total substorm dissipation.

The source of the energy flow reaching the Earth is the Sun, which undergoes long-term and short-term changes. These changes together with their effects on the Earth are called space weather. Space weather conditions vary together with the varying Sun's activity. Thus, also substorm properties and energetics show differences between low and high solar activity phase. These differences were studied by comparing substorms occurring in 1997 and 1999. Furthermore, substorms were divided into several subclasses, for example into isolated and stormtime substorms, which were examined separately.

Publishing unit
Geophysical Research

Classification (UDC)
52-85; 523.62; 523.98; 533.9.98; 537.872

Key words
Space plasma physics, magnetosphere, ionosphere magnetic substorms, magnetic energy, space weather

ISSN and key name
0782-6117 Finnish Meteorological Institute Contributions

ISBN
951-697-558-5(print), 952-10-0423-1(pdf)

Language
English

Pages
150

Price

Sold by
Finnish Meteorological Institute Library
P.O. Box 503
FIN-00101 Helsinki, Finland

Note

Julkaisija
Ilmatieteen laitos
PL 503
00101 HELSINKI

Julkaisun sarja, numero ja raporttikoodi
Contributions 36, FMI-CONT-36
Julkaisuaika
Maaliskuu 2002

Tekijä(t)
Eija I. Tanskanen

Projektin nimi	Toimeksiantaja

Nimeke
Magneettiset alimyrskyt osana magnetosfäärin energiataloutta

Tiivistelmä
Tässä väitöskirjassa tutkitaan magneettisia alimyrskyjä. Väitöskirja koostuu johdanto-osasta ja viidestä tieteellisestä artikkelista. Johdannossa käsitellään alimyrskyjen energiataloutta ja alimyrskyjen ominaisuuksia, joiden tarkemmista yksityiskohdista antavat lisävalaistusta tieteelliset artikkelit.

Aurinkotuulessa on valtava määrä energiaa, josta vain noin 1% kulkeutuu Maan magnetosfääriin. Magneettiset alimyrskyt, joita esiintyy keskimäärin muutamia kertoja päivässä, ovat tärkeässä roolissa energian kuljettamisessa aurinkotuulesta Maan magnetosfäärin ja ionosfäärin muodostamaan systeemiin. Magnetosfäärin eniten energiaa kuluttavat mekanismit ovat ionosfäärin Joulen lämmitys, elektronien sataminen ionosfääriin, hiukkasinjektiot rengasvirtaan ja magnetosfäärin pyrstön prosessit kuten plasmoidin muodostuminen sekä plasmalevyn lämmitys. Tilastolliset tulokset yli 800:sta alimyrskystä osoittavat, että ionosfäärin energiakulutus, pääasiassa, Joulen lämmityksenä, kattaa yli puolet alimyrskyjen kokonaiskulutuksesta.

Maahan kulkeutuva energia on lähtöisin Auringosta, jossa tapahtuu jatkuvasti lyhytaikaisia ja pitkäaikaisia muutoksia. Näitä muutoksia yhdessä niiden Maalle aiheuttamien vaikutusten kanssa sanotaan avaruussääksi. Muutokset avaruussäässä aiheuttavat muutoksia magnetosfäärin alimyrskyaktiivisuudessa. Alimyrskyjen välisiä eroja tutkittiin vertailemalla vuoden 1997 ja 1999 alimyrskyjä. Lisäksi tutkittava alimyrskydatajoukko jaettiin kolmella muulla tavalla, esimerkiksi rauhallisen ajan ja myrskyajan alimyrskyihin, joita kaikkia tutkittiin erikseen.

Julkaisijayksikkö
Geofysiikka

Luokitus (UDK)	Asiasanat
52-85, 523.62, 523.98, 533.9.98, 537.872	Avaruusplasmafysiikka, magnetosfääri, ionosfääri magneettiset alimyrskyt, magneettinen energia, avaruussää

ISSN ja avainnimeke	ISBN
0782-6117 Finnish Meteorological Institute Contributions	951-697-558-5(print), 952-10-0423-1(pdf)

Kieli	Sivumäärä	Hinta
englanti	150	

Myynti	Lisätietoja
Ilmatieteen laitos, kirjasto PL 503, 00101 HELSINKI	

PREFACE

The work constituting the basis for this thesis has been performed at the Geophysical Research Division (GEO) of the Finnish Meteorological Institute (FMI), at the Goddard Space Flight Center (GSFC) at Greenbelt, USA and at the Department of Physics of the University of Helsinki. I wish to thank the Directors of these institutions for providing excellent working conditions. This study was financially supported by the Academy of Finland, the NASA Goddard Space Flight Center and the Finnish Graduate School in Astronomy and Space Physics, as well as by grants from Vilho, Yrjö and Kalle Väisälä foundation of the Academy of Finland.

I would like to warmly thank my supervisors Prof. Hannu Koskinen and Prof. Tuija Pulkkinen for their continuous support during the course of this work. My special thanks go to Hannu Koskinen who recruited me to the GEO, who taught the basics of the Space Plasma Physics and who originally proposed this topic to me. I am also grateful to Tuija for teaching me to write scientific papers and for guiding me smoothly to the international seas of space physics.

I am also grateful to Prof. Risto Pellinen, head of the Department of Geophysics, Dr. Risto Pirjola, head of the Space Plasma Physics Division, and Prof. Tuija Pulkkinen, former head of the Space Plasma Physics Division, for making the GEO such a good and flexible place to work in. I thank the entire staff of the GEO for the support they have provided for this work. Numerous scientific and non-scientific discussions have enriched my working days. I would particularly like to thank Ari Viljanen and Kirsti Kauristie, as P.I.s of IMAGE and MIRACLE, for making the data easily usable. This thesis would also look quite different without Lasse Häkkinen's help with computers and Teemu Mäkinen's help with illustration. I also want to thank the GEO's Säh(el)ly(s)-team and Geodynamo music group for refreshing breaks during the working days.

I wish to thank Dr. Jim Slavin, head of the Electrodynamic Branch of the Laboratory for Extraterrestrial Physics, for his hospitality during my two visits to the GSFC. His constructive comments, also by e-mail, have helped me understand the magnetospheric processes, especially those in the far-tail. I would also like to thank Adam Szabo, Chin-Chun Wu, Don Fairfield, Michael Collier, Jesper Gjerloev and Richard Vondrak for invaluable discussions during the visits.

I further thank Dr. Eigil Friis-Christensen and Prof. Kalevi Mursula for careful reading of my manuscript and for their interest in this thesis.

I also extend my gratitude to several other co-workers: Emilia Huttunen at the University of Helsinki, Jouni Jussila at the University of Oulu, Nikolai Ostgaard at the University of Berkeley, Aki Ieda at the University of Kyoto and Anatoli Petrukovich at the IKI Space Research Institute. Outside work my thanks go to Virpi Koivu for explaining the weird philosophy of the English language, over and over again, as well as to my family and friends.

Lastly, I thank my dearest husband Antti. He is my daily proof of that there is something even more important than terrestrial substorms.

Helsinki, February 2002

Eija Tanskanen

Contents

List of publications

A list of publications (reprinted after the introductory part), which are included to this thesis:

(I) Kallio, E.I., T.I. Pulkkinen, H.E.J. Koskinen, A. Viljanen, J.A. Slavin, and K. Ogilvie, Loading-unloading processes in the nightside ionosphere, Geophys. Res. Lett., 27, 1627, 2000;

(II) Petrukovich, A.A., E.I. Kallio, T.I. Pulkkinen, H.E.J Koskinen, Solar wind energy input and magnetospheric substorm activity compared, in Proceedings of the 5th International Conference on Substorms (ICS-5), St. Petersburg, Russia, 16-20 May, ESA SP-443, 67, 2000;

(III) Tanskanen, E., H.E.J. Koskinen, T.I. Pulkkinen, J.A Slavin, and K. Ogilvie, Dissipation to the Joule heating: Isolated and stormtime substorms, Adv. Space. Res., in press, 2002;

(IV) Tanskanen, E.I., A. Viljanen, T.I. Pulkkinen, R. Pirjola, L. Häkkinen, A. Pulkkinen, and O. Amm, At substorm onset, 40% of AL comes from underground, J. Geohys. Res., 106, 13119, 2001;

(V) Tanskanen, E., T.I. Pulkkinen, H.E.J. Koskinen, and J.A. Slavin, Substorm energy budget during low and high solar activity: 1997 and 1999 compared, J. Geophys. Res., in press, 2002.

Summary of publications

(I) The first publication deals with the magnetospheric loading-unloading processes during isolated substorm events. The substorms are examined using the IL index derived from the IMAGE magnetometer measurements. Magnetospheric energy input and ionospheric Joule dissipation is computed for each event using the time integrals over the entire substorm periods.

(II) The second publication studies the isolated and stormtime auroral substorms during 1997 in terms of energy input and ionospheric Joule heating. Furthermore, reliability of epsilon measurements is analyzed using two-point measurements in the solar wind.

(III) The third publication analyzes the energy input for 1997 substorms using epsilon and transverse epsilon parameters. Energy input and Joule dissipation is correlated using those two different coupling parameters.

(IV) The fourth publication analyzes external and internal contributions to the magnetic variations measured at the Earth's surface. Superposed epoch analysis is used to illustrate the induction effect during different substorm phases.

(V) The fifth publication compares substorm energy budget during the quiet year 1997 and during the active year 1999. Events during both years, total amount 839, are investigated using following measures: number, onset time, duration, latitude, intensity, energy input and Joule dissipation.

The author is responsible for the major work in the first, the third, and the fifth paper: event selection, programming, analysis and writing. In the second paper half of the work was done by the author herself and in the fourth paper the author was responsible for the event selection and the superposed epoch analysis.

Chapter 1

Introduction

The interplanetary space is not empty. It is filled with fields, matter, energy, and activity often invisible to the eye. The charged particles and the magnetic field originating from the Sun form the solar wind (SW) and interplanetary magnetic field (IMF). While light travels from the Sun to the Earth in about 8 minutes, the solar wind usually reaches us in 3 or 4 days. The solar wind carries energy to the terrestrial and other planetary magnetospheres. The only visual sign of the solar wind energy ending up into the magnetosphere is auroral light.

In the Earth's magnetosphere, the solar wind energy is dissipated into various sinks during magnetic storms and substorms. The main energy dissipation channels are the ring current encircling the Earth at the equatorial plane, the ionospheric Joule heating, auroral precipitation, plasma sheet heating in the nightside magnetosphere, and release of plasmoids from the magnetospheric tail. About half, perhaps even a larger part, of the energy ends up in the ionosphere, of which the Joule heating consumes the main part.

The Sun, the source of the energy flow reaching the Earth, undergoes long-term variations such as the roughly 11-year solar cycle. Moreover, the Sun undergoes temporally and spatially limited changes such as the solar flares and coronal mass ejections (CME). The Sun's long-term and short-term changes and their effects on the Earth are commonly called space weather. During recent years, space weather research has become a popular subfield of solar-terrestrial physics as its technological consequences have become increasingly important.

There are hundreds of active satellites in the near-Earth space and the International Space Station (ISS) is continuously manned. The Sun may

be hazardous for satellites, astronauts and ground-based systems in various ways: (1) Radiation doses and electrical charging of satellites in the near-Earth space may damage critical spacecraft components and functions and be fatal to human beings in space; (2) Disturbances in the ionosphere may degrade the performance of navigation and communication systems; (3) The ionospheric currents related to the ionospheric disturbances generate electric fields on the ground, which may interfere with the operations of large-scale power distribution grids.

The most important social and economic aspects of space weather are related to being aware of and trying to avoid the consequences of space weather events. Avoiding hazardous space weather events is possible either by system design or by efficient warning and prediction systems allowing for preventive measures to be taken. Only in the U.S. have the social and economic losses from space weather disturbances been estimated to amount tens of millions of dollars each year. In order to build efficient warning systems, intensive research on solar wind-magnetosphere-ionosphere (SMI) system are needed. One important component in such research is the energetics of the SMI system, in particular the role of substorms as a part of global energy flow, which is the topic of the present thesis.

1.1 Terrestrial magnetosphere and ionosphere

The terrestrial magnetosphere (figure 1.1) is a vast plasma cavity around the Earth, which is created by electrodynamic interaction between the solar wind and the Earth's magnetic field. The discovery of the magnetosphere was closely related to the discovery of the solar wind. In the early 1930's, *Chapman and Ferraro* [1931, 1932, 1933] suggested that neutral plasma clouds would leave the Sun and affect the geomagnetic field. The term magnetosphere was coined some 30 years later by *Gold* [1959a, 1959b]. This occurred when the first space programs were introduced.

The Earth has an internal dipole magnetic moment of $8{\cdot}10^{22}$ Tm^3 that produces on the Earth's surface a magnetic field of about 30 000 nT at the equator and about 60 000 nT at the poles. The solar wind compresses the sunward side of the magnetosphere to a distance of typically 10 Earth radii (R_E) and it drags the night-side magnetosphere out to some 1000 Earth radii. The magnetosphere is a complex, dynamic and fluctuating system and the physical mechanisms and processes driving the magnetosphere are not fully known. However, the variable properties of the solar wind are known to play an essential role in the dynamics of the magnetosphere.

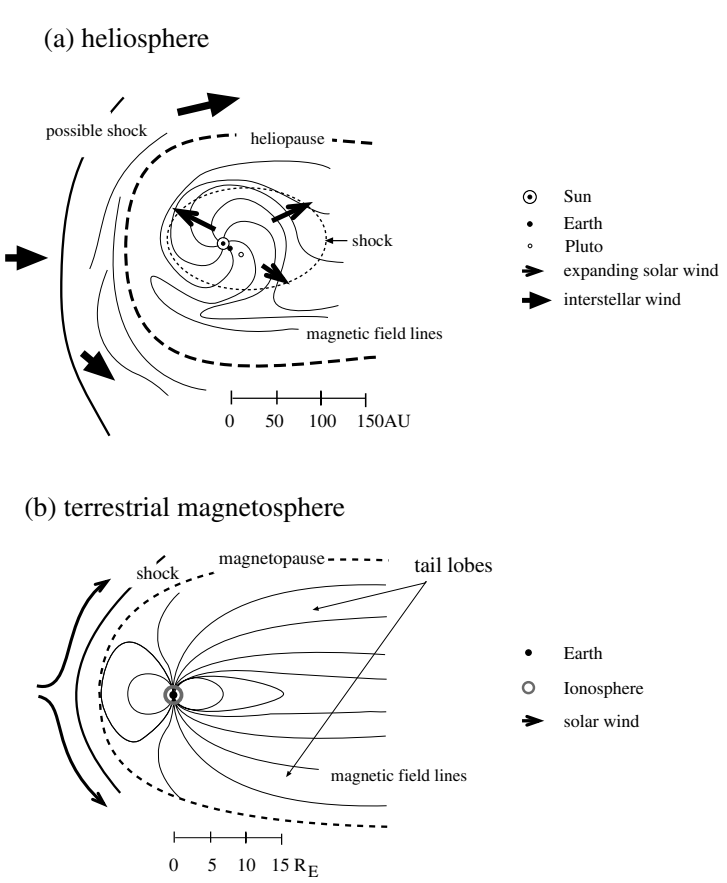

Figure 1.1: Sketches of (a) heliosphere, and (b) terrestrial magnetosphere. Heliosphere has been drawn in an ecliptic plane and magnetosphere in a noon-midnight plane.

The magnetosphere is bounded from below by the ionosphere, which is an electrically conducting part of the upper atmosphere, from roughly 80 to 1000 km above the Earth's surface. The ionosphere may be said to have been discovered by Balfour Stewart in 1882, when he wrote an article titled "Terrestrial Magnetism" for Encyclopaedia Britannica, in which he concluded that the upper atmosphere was the most probable location for the electric currents that produce solar-controlled variations in the magnetic field measured on the Earth's surface. The existence of the ionosphere was verified in 1925 when short pulses of radio waves were used to locate the altitude of the electrically reflecting layer.

Ionospheric electric fields are the main result of the coupling between the magnetosphere and the ionosphere. While at low latitudes the ionospheric plasma is co-rotating with the Earth, at higher latitudes it is convecting under the influence of the large-scale magnetospheric electric field created by the solar wind-magnetosphere interaction. Ionospheric currents flow along the auroral oval so that two convection electrojets are formed at the altitude of about 100 km: eastward electrojet on the duskside and westward electrojet on the dawnside.

Maintaining the average magnetosphere-ionosphere (MI) configuration consumes a significant amount of energy. It has been estimated that the maintenance of the long magnetotail requires roughly $(2\text{–}3)\cdot 10^{11}$ W, which is much less compared to what is available in the solar wind. If all particles incident on the dayside magnetopause gave up their entire kinetic energy, the obtained power would be of the order of 10^{13} W. A vast majority of this energy passes by the Earth while only a small fraction is used to maintain the Earth's magnetosphere and further dissipates to the magnetospheric and ionospheric sinks (see Chapter 2).

1.2 Measurements

Our current knowledge about the magnetosphere, its coupling to the ionosphere, and different realizations of geomagnetic activity, is primarily a result of satellite measurements of the magnetosphere as well as of long-term ground-based observations of the ionosphere.

One of the first scientific magnetometer was designed by C.F. Gauss in 1832. It was a simple variometer consisting of a permanent bar magnet suspended horizontally by a gold fiber. Nowadays there are several arrays of magnetometers around the world covering both hemispheres (Appendix A). Most ground-based magnetometers are located in the northern high-latitude region, between latitudes 55° and 75°. Ten to thirteen magnetometers out of about 200 northern hemisphere magnetometers are selected to form a global magnetometer chain, the *AE* chain, which is widely used, e.g., in parameterizing the high-latitude ionospheric magnetic activity. However, the latitudinal coverage of the *AE* chain is not sufficient for detecting auroral electrojets located at very high or very low latitudes. Longitudinal magnetometer chains, covering certain limited longitude range, represent the ionospheric activity better in this range than the *AE* chain. The five most important longitudinal chains are the IMAGE array in Fennoscandia [*Syrjäsuo et al.,* 1998], network 210 MM coordinated by Japan, CANOPUS

in Canada [*Rostoker et al.,* 1995], the Danish Meteorological Institute (DMI) chain along the east and west coasts of Greenland and MAGIC on the Greenland ice cap [*Stauning et al.,* 1995]. Data from these chains are used for the purpose of this thesis work, but the focus is on the IMAGE magnetometer chain which is part of the ground-based MIRACLE (Magnetometers - Ionospheric Radars - Allsky Cameras Large Experiment) network, containing 25 magnetometers sampling at 10-s resolution (see the location of the stations in Appendix A).

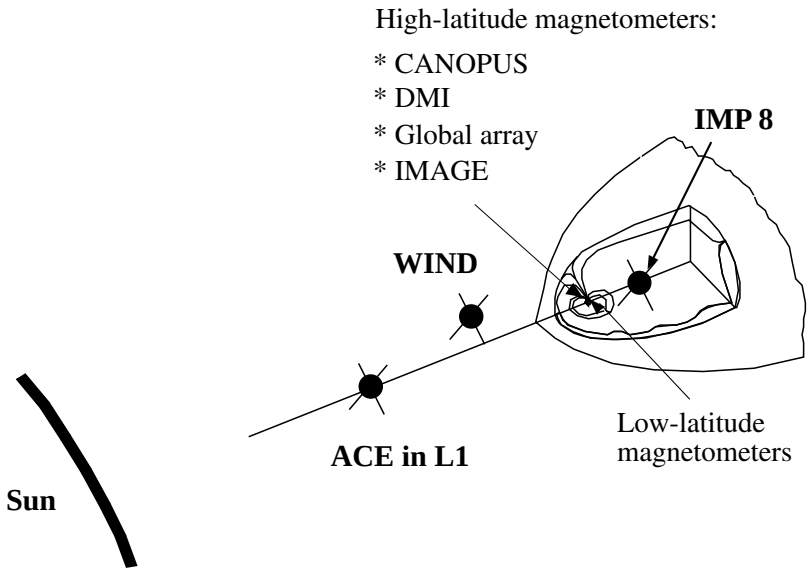

Figure 1.2: Space-borne and ground-based observations used in this thesis work.

The first scientific satellites were launched during the International Geophysical Year (IGY) 1957-1958. The successful launch of Sputnik I demonstrated the ability of mankind to send a satellite to orbit the Earth. Explorer I, launched in 1958, returned data and made it possible to start the observation of changes in the Earth's magnetic environment. Around 1965, satellites began to record changes in the Earth's magnetic tail that are related to substorms. The International Solar Terrestrial Program (ISTP) continues the scientific spacecraft era by providing a good opportunity to study the global geomagnetic activity using multiple spacecraft. One goal of the ISTP is to carry out simultaneous satellite measurements in various regions of the terrestrial magnetosphere and in the neighboring interplane-

tary space. The ISTP contains several satellites of which WIND and ACE are used for this thesis. Additional data from NASA's IMP 8 satellite is used to supplement the data from the ISTP missions.

The WIND spacecraft was launched in November 1994. It has a complex petal-shaped orbit carrying it out to about 200 R_E upstream of the Earth. ACE was launched in August 1997, and it orbits the Lagrangian libration point L1 which is a point of Earth-Sun gravitational equilibrium. The L1 point lies at about 235 R_E from Earth in the direction of the Sun. In this thesis the WIND Magnetic Field Instrument (60-s resolution, MFI) [*Lepping et al.,* 1995] and Solar Wind Experiment (92-s resolution, SWE) [*Ogilvie et al.,* 1995] are used together with the ACE Magnetic field experiment (16-s resolution, MAG) [*Smith et al.,* 1998] and the Solar Wind Electron Proton Alpha Monitor (64-s resolution, SWEPAM) [*McComas et al.,* 1998]. IMP 8, launched already in 1973, is in a nearly circular orbit surrounding the Earth with a radius of 35 R_E. While the spacecraft spends approximately 4 days of its 12.5-day orbit in the Earth's magnetosheath and magnetotail, it is in the solar wind for the remaining time. IMP 8 ceased its operation at the end of 2000. For the purposes of this thesis, IMP 8 is used to investigate the local homogeneity of the solar wind, and to seek signatures of plasmoids in the magnetotail.

1.3 Geomagnetic activity

1.3.1 Substorms and storms

Magnetic storms and substorms are the two main appearances of geomagnetic activity. The term magnetic storm was coined by Alexander von Humboldt (1769-1859) who set up a network of magnetic observatories across the Russian empire, in co-operation with the Czar, to show that there were identical geomagnetic disturbances all over the world.

The magnetic storms are the strongest geomagnetic variations caused by the Sun, producing 50–300 nT changes in the Earth's magnetic field at the equator. Magnetic storms often begin with a sudden global increase in the value of geomagnetic field, which is followed by a rapid decrease of the horizontal component during the storm main phase. Storms end with a slow recovery phase which may last from one to several days. During stormy days the energy content of the ring current increases to unusually large values, which is the main reason for the equatorial field suppression.

The first reported observations of substorm-like features were made in 1838 by E.C. Herrick [*Siscoe,* 1980]. From the beginning of the 20th cen-

tury, Birkeland observed these conspicuous magnetic signatures and suggested that there was a new type of magnetic activity, a polar elementary magnetic storm which is nowadays known as a magnetospheric substorm [*Birkeland,* 1908; *Boström,* 1964]. Various names have been used for substorms throughout the history: polar elementary magnetic storm, magnetic bay [*Chree,* 1911, 1912], auroral substorm [*Akasofu and Chapman,* 1961], or simply substorm. At the beginning of the substorm research era, substorms were thought to be building blocks of magnetic storms. However, a substorm can occur either during magnetic storms (to be called stormtime substorms, SS), or independent of storms (isolated substorms, IS). These two classes of substorms are quite different from each other in terms of numbers, intensities and energies, as will be shown in Section 4.1.

A substorm can be defined as a transient process initiated on the nightside of the Earth, in which a significant amount of energy, derived from the solar wind-magnetosphere interaction, is deposited in the auroral ionosphere and in the magnetosphere [*McPherron,* 1979]. *Rostoker et al.* [1980] lists some phenomena accompanied with substorms: (1) increase in auroral luminosity in the midnight sector, (2) Pi 2 pulsation bursts, (3) intensification of the westward electrojet, and (4) a westward traveling surge.

An important linkage between the solar wind and the magnetosphere was discovered by *Fairfield and Cahill* [1966]. They noticed that the level of magnetospheric storminess depends strongly on the IMF Z-component given in geocentric solar magnetospheric (GSM) coordinates (Appendix B). Consequently, the substorm sequence, carrying solar wind energy to the Earth, is thought to begin when a southward turning of the *IMF* activates dayside reconnection [*Russell and McPherron,* 1973; *Baker et al.,* 1984; *Baker,* 1996]. In this thesis, substorms are defined as intervals of increased energy dissipation into the auroral ionosphere, which is determined on the basis of the westward auroral electrojet (Papers I–V). Properties of substorms have been studied over 40 years, since the beginning of the space era. Landmark papers were *Akasofu* [1964] and *Akasofu et al.* [1965], which defined the substorm sequence of events from the ground-based observer's point of view. Since those times, the understanding of substorms has considerably improved, but we still do not know all the important parameters. The typical duration, frequency, intensity and size characterizing substorms are studied in Chapter 3.

Substorms play an important role in magnetospheric energetics, in yearly averages even more important than the magnetic storms, although the latter are much more intense. Substorms are known to cause 100–2500 nT changes in the Earth's magnetic field at high latitudes, which is 0.2–4% of the normal

magnetic field. Magnetic substorms take place when the IMF is slightly southward (about 5 nT) for an hour or so, whereas magnetic storms develop when the IMF is strongly southward for a prolonged period, for several hours [*Gonzalez and Tsurutani,* 1987]. The only visible signs of magnetic storms and substorms, the aurora, are seen in the northern (Aurora Borealis) and southern (Aurora Australis) auroral regions.

1.3.2 Geomagnetic indices

Geomagnetic activity is often described by geomagnetic indices [*Mayaud* 1980]. Geomagnetic indices are widely used for research in geomagnetism, aeronomy, and solar-terrestrial physics. Indices can be used to identify the substorms and to measure their properties, such as intensity, duration, frequency, or Joule dissipation. In addition, indices can be correlated with other parameters, for example with solar wind measurements. When correlations are found, the SW parameters can be used to estimate or predict the development of magnetospheric phenomena.

Dst is a geomagnetic index which has been used to characterize the worldwide magnetic storm levels on an hourly basis since 1957 [*Sugiura,* 1964; *Sugiura and Kamei,* 1991]. It is constructed by averaging the horizontal component of the geomagnetic field by using low- and mid-latitude magnetograms. The stations used for the official *Dst* index are Kakioka (KAK), Honolulu (HON), Hermanus (HER) and San Juan (SJG). Alternative selection of stations have also been used for specific studies (e.g. *Häkkinen et al.* [2002a, 2002b]). The *Dst* index responds most strongly to the ring current and to the magnetopause current [*Rangarajan,* 1989; *Burton et al.,* 1975].

The auroral electrojet (AE) indices were originally introduced as measures of global electrojet activity [*Davis and Sugiura,* 1966]. The AE indices are derived from geomagnetic variations in the horizontal component, observed at selected (10-13) observatories along the auroral zone in the northern hemisphere. The term "AE indices" combines four indices: AU, AL, AE, and AO. The strength of the westward and eastward auroral electrojets are reflected in AL and AU, respectively. The third electrojet index, the AE index, corresponds to the difference between the AU and AL envelopes i.e. $AE = AU - AL$, and the fourth, the AO index, provides a measure of the equivalent zonal current ($AO = (AU + AL)/2$). Several local electrojet indices have been created because of their better coverage of maximum disturbances or faster data retrieval. Examples of local indices are the CU/CL indices from the CANOPUS data [*Rostoker,* 1995] and the IU/IL indices from the IMAGE data (Papers I–V).

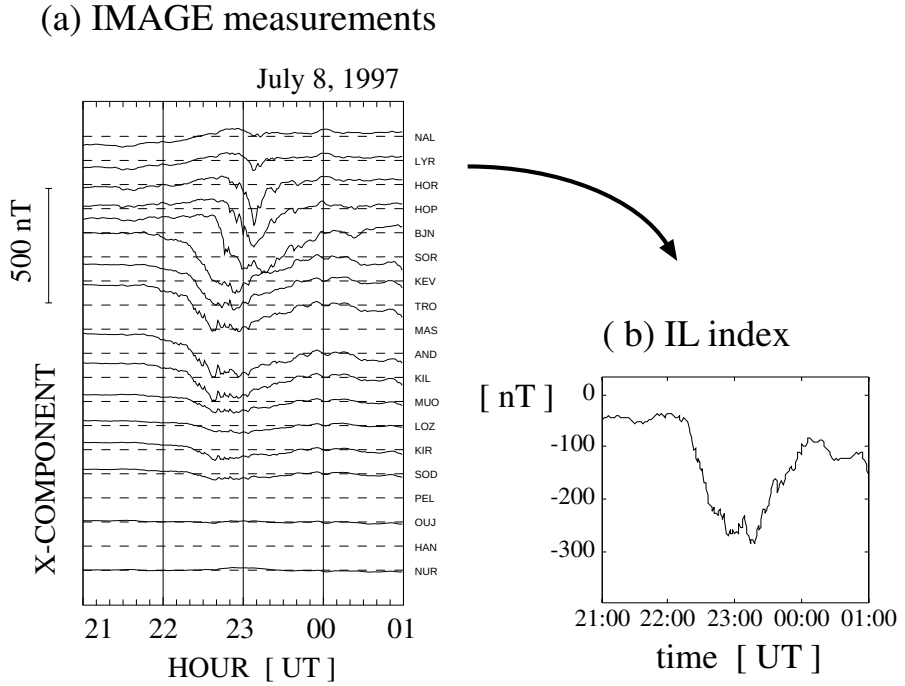

Figure 1.3: Method to compute the IL index. The IL index was constructed by taking the minimum of the north-south components, which were measured in the IMAGE chain magnetometer stations.

The IL index was constructed by computing the envelope of the north-south components of the IMAGE magnetometer stations. The baselines, necessary for the envelope computation, were visually selected from the IMAGE data. The most quiet time period during each day, lasting at least 30 min, was selected to determine the baseline. If there were no quiet periods on some day, the data of the previous day was used.

1.3.3 Substorm phases

A substorm consists of three different phases: the growth phase (GP), the expansion phase (EP) and the recovery phase (RP) [*Akasofu,* 1968; *McPherron,* 1970] (figure 1.4). A substorm starts with a growth phase when the energy transfer from the solar wind to the magnetosphere is enhanced. This happens when the *IMF Z*-component turns negative. Part of the solar wind energy flows directly through the magnetosphere and part of it is stored in

the form of magnetic energy in the lobes of the magnetotail. *McPherron* [1968] noted that, during a substorm growth phase, there is an increased probability to observe localized auroral activations such as pseudobreakups [*Akasofu* 1964]. The features distinguishing pseudobreakups from substorms are their short duration (less than 10 minutes) and small intensity (less than 100 nT) [*McPherron,* 1991].

The substorm expansion phase starts with an onset, which is the moment of time of a sudden enhancement of the westward electrojet. The energy loaded earlier is released during the expansion phase, while the main part of the energy feeding the substorm is still coming directly from the solar wind (Paper I). At the end of the expansion phase, the IL index reaches a minimum and begins to recover towards the quiet time level near zero. During the recovery phase, the magnetosphere returns back to its quiet-time state, which is nevertheless not totally quiet, but merely less disturbed than storm and substorm times. Even an isolated substorm is a complex set of phenomena, and its different phases are rarely easily distinguishable. For example, several new intensifications may occur during a substorm recovery phase. These may be considered to start a new substorm or belong to the earlier substorm as extra intensifications. In this study, a new substorm is considered to begin when the IL index has returned near zero two hours before the beginning of the event.

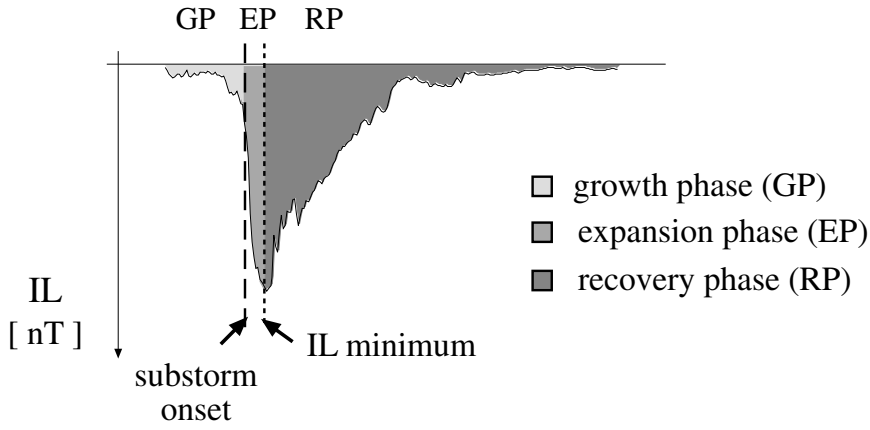

Figure 1.4: A sketch of substorm phases.

1.4 Energy transfer mechanisms: reconnection and dynamo action

The magnetic field shields the Earth from a direct bombardment by solar wind particles. However, the shield is rather leaky, allowing solar wind plasma to penetrate into the magnetosphere. The leakage is mainly due to a large-scale reconnection process which may occur in collisional plasma when the field geometry has a sufficiently large antiparallel magnetic field configuration. At neutral points where the field's direction is undetermined (B = 0), two field lines can interconnect. This may happen at the dayside magnetopause when the IMF is strongly southward, and in the tail of the magnetosphere (figure 1.5). Furthermore, it may take place in the vicinity of the cusp and at the dawnward and duskward flanks of the magnetopause [*Le et al.,* 1996].

The idea of reconnection was introduced by *Giovanelli* [1947] who was convinced of the importance of the neutral points for solar flares. Dungey was the first to apply it to the magnetosphere [*Dungey,* 1953, 1961]. Much later, reconnection was verified quantitatively at the dayside magnetopause [*Paschmann,* 1979]. At the dayside magnetopause, reconnection changes the magnetic topology so that closed geomagnetic field lines become connected to the IMF, allowing the solar wind energy to flow into the magnetosphere. The reconnected field lines are swept along by the solar wind to the nightside, until the increasing magnetic tension leads to a second reconnection process in the tail. Not all factors controlling the reconnection rate are fully understood, but at least the magnitude of the IMF southward component is known to be critical for dayside reconnection.

Reconnection is a process converting magnetic energy into kinetic energy ($\mathbf{j} \cdot \mathbf{E} > 0$). In the tail, the reconnection surplus magnetic energy of the high-latitude tail lobes is converted into the kinetic energy of particles. This newly released kinetic energy accelerates the tail-to-ionosphere plasma flow [*Stern,* 1984]. Correspondingly, a process converting kinetic energy into the magnetic energy ($\mathbf{j} \cdot \mathbf{E} < 0$) is also needed. However, only a small part of the solar wind kinetic power flowing through the cross sectional area of the magnetosphere needs to be converted into energy dissipated inside the magnetosphere in order to maintain the magnetosphere and also in order to be enough to all known magnetospheric sinks. Conversion from kinetic energy to the magnetic energy requires a generator in some part of the system. Such a generator, or dynamo, is assumed to exist at least in the magnetotail boundary [*Stern,* 1984]. It has also suggested that the dynamo

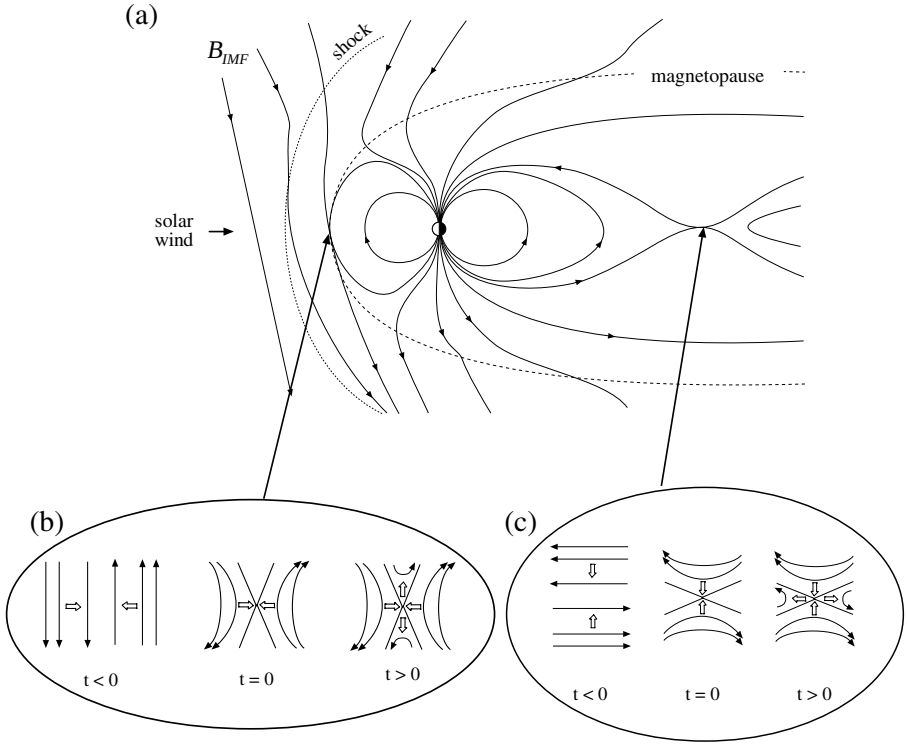

Figure 1.5: (a) Plasma flow from the solar wind to the magnetosphere and to the ionosphere, driven by magnetic reconnection. (b) Magnetopause reconnection. (c) Magnetotail reconnection.

exists in the dayside magnetopause [*Song and Lysak,* 1989]. In addition, *Song and Lysak* [1989] have speculated that the dynamo is effective if the levels of fluctuations, irregularities and non-linearity are high enough in the reconnection region.

1.5 Database

The full data set examined in this thesis includes 839 substorm events covering the period from January 1, 1997, to December 31, 1997, and from January 1, 1999, to November 30, 1999. During those periods both magnetic field and solar wind velocity data were available either from the WIND or ACE spacecraft. The WIND spacecraft MFI and SWE instruments were used in 1997, and ACE spacecraft MAG and SWEPAM instruments in 1999.

Only substorms occurring between 1600 UT and 0200 UT were selected to the database, because during this period IMAGE is situated at the nightside, where the largest effects of the substorms are seen [*Akasofu,* 1964; *Caan et al.,* 1978], and where IL index thus gives a good estimate of the AL index [*Kauristie et al.,* 1996].

1.5.1 Method of identifying substorms

The method of identifying substorms was the following:

(1) The midnight sector proxy of the westward electrojet index AL, which we call the IL index, was constructed from IMAGE magnetic field observations.

(2) The magnetospheric energy input was computed using an empirical coupling function, the ϵ-parameter, to be described in detail in the following chapter.

(3) The substorms were identified from the IL index. All substorms with IL less than –100nT were selected into the database.

(4) The solar wind time series were shifted to account for the time delays, ΔT, from WIND or ACE to the coupling region ($X(GSM) = 10\ R_E$) by $\Delta T = \Delta\ X/V$, where V is the average speed observed during the substorm.

(5) The main onset of a substorm was the time when the IL index showed a rapid decrease, about 100 nT in 30 minutes, that led to a negative bay development.

(6) The beginning of the substorm growth phase was defined as the moment of the IMF southward turning. If there were several southward turnings, the nearest one to the onset was selected.

(7) The event was considered to end when IL returned back to the quiet level values, close to zero, after the recovery phase.

(8) Substorms were categorized to the isolated (stormtime) substorms if the Dst index was larger (lower or equal) than –40 nT during the event.

1.5.2 Sample interval: January 9 – 11, 1997

A three-day period of moderate solar magnetic and geomagnetic activity is presented in figure 1.6 to give an example of storm and substorm events. The first panel shows the Dst index illustrating the worldwide magnetic storm level. The index was nearly zero until the beginning of January 10 when a pressure pulse was observed. The pressure pulse, which caused dayside compression of the magnetopause, is indicated by a slight rise in Dst.

Thereafter, Dst decreased to –78 nT in five hours, indicating an increase in the ring current (RC) around the Earth.

The second panel shows the global AL index illustrating substorm activity in the auroral zone (between 55° and 75°). Substorms can be identified from the AL data as negative bays lasting typically about four hours (Paper V). The determination of the exact beginning and end of the substorms is not unique and determination becomes even more complicated when the global activity level is high. For the purpose of subtorm determination, local indices are shown in figure 1.6c. Most substorms are more intense and their onsets sharper in local indices than in global indices. This is because the local indices have a better ability, than the AE index, to catch auroral activity at higher (about 80°) or lower (about 60°) latitudes. Individual substorm events are marked with grey shading in the figure.

Substorms take place during both quiet and stormy periods. In total, twelve substorms were identified in figure 1.6c, of which nine were isolated and three stormtime events, when the Dst-limit –40 nT was used to separate isolated and stormtime substorms. Thus, during this three-day period, isolated events were more numerous than stormtime events. This result was confirmed by a large statistical study (Paper I and Paper V). It is also obvious that the stormtime substorms are more intense than their isolated counterparts. Only few additional substorms would have been identified if other longitudinal chains, e.g., Greenland's chains, would have been used for substorm identification.

The solar wind velocity varied between 350 km/s and 550 km/s, being on average 400 km/s before the storm and 450 km/s during the storm. In the statistical study, high speeds were related to CMEs or events called "high speed streams". In this event, WIND observed a shock, driven by a CME, starting on January 10 at 00:22 UT. It is clear that the variations in storm and substorm activity are clearly synchronized with the $IMF\ B_z$ variations as discussed previously.

The energetics of the twelve substorms presented here and the energetics of other 827 substorms in 1997 and 1999 are examined in the following chapter.

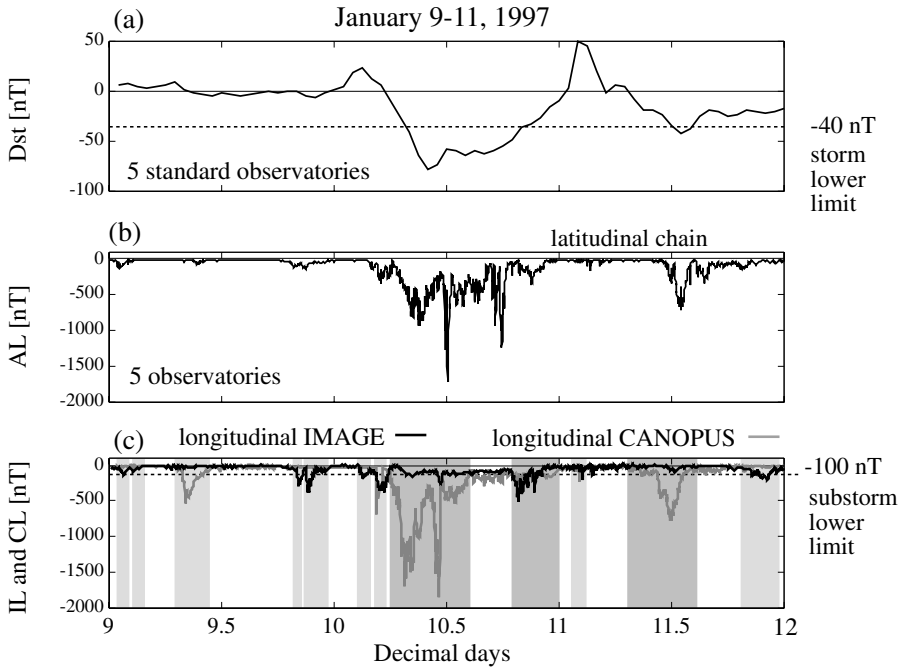

Figure 1.6: Sample interval: January 9 – 11, 1997. Stormtime substorms are marked with dark grey shading and isolated substorms with light grey shading.

Chapter 2

Substorm energetics: source and sinks

This section is focused on the energetics of the SMI system, i.e., the energy input from the solar wind and dissipation in the ionosphere and magnetosphere. The total energy budget of magnetospheric substorms and the relative importance of the different dissipation channels are studied. Single-event studies on magnetospheric and ionospheric energy sinks during substorms [*Akasofu,* 1981; *Weiss et al.,* 1992; *Pulkkinen et al.,* 2002] and storms [*Lu et al.,* 1998; *Knipp et al.,* 1998; *Turner et al.,* 2001] have been conducted in several earlier papers. However, only few quantitative studies have been made on the total energetics of substorms (Paper V) or the relative importance of different energy sinks during substorm events [*Østgaard et al.,* 2002; *Østgaard and Tanskanen,* Energetics of isolated and stormtime substorms, submitted]. The main ionospheric sinks are Joule heating and auroral precipitation, which both are examined in section 2.2. The energetics of the main magnetospheric sinks, ring current, plasmoid release, and plasma sheet heating, are estimated in section 2.3. The energy dissipation in the post-plasmoid plasma-sheet (post-PPS) is included in the plasmoid estimates.

2.1 Solar wind energy input

2.1.1 Epsilon parameter

The solar wind is the primary source of energy that drives dissipative processes in the Earth's magnetosphere and ionosphere. There is still no theoretically correct and empirically satisfactory coupling function between the

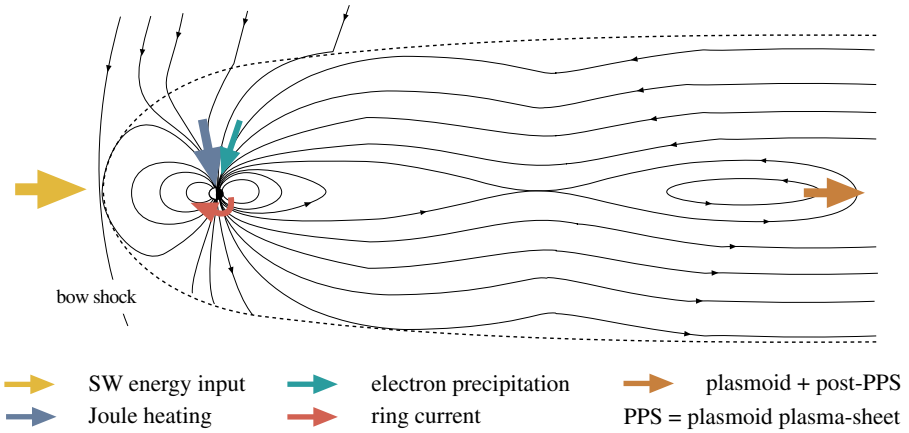

Figure 2.1: Substorm energetics: source and sinks.

solar wind parameters and the geomagnetic activity. One of the earliest and most widely used coupling functions is Akasofu's epsilon parameter [*Perreault and Akasofu,* 1978; *Akasofu,* 1981] which is constructed on the basis of a dimensional analysis: The epsilon parameter is a product of the Poynting flux of the IMF (in SI units),

$$\mathbf{S} = \frac{1}{\mu_0}(\mathbf{E} \times \mathbf{B}), \tag{2.1}$$

and the effective size of the area through which the Poynting flux enters the magnetosphere,

$$\sin^4(\theta/2) \cdot 4\pi l_0^2, \tag{2.2}$$

where $\mathbf{E}$ is the interplanetary electric field, $\mathbf{B}$ the interplanetary magnetic field, μ_0 the permeability of free space, θ the IMF clock angle ($\tan\theta{=}B_y/B_z$) in geocentric solar magnetospheric (GSM) coordinates, and l_0 an empirical parameter to fit the average energy input to the average estimated output. Substituting the electric field, $\mathbf{E} = -\mathbf{v} \times \mathbf{B}$, in formula (2.1) gives the epsilon [*Akasofu* 1981; *Kan et al.* 1980; *Kan and Akasofu* 1982] in SI units as

$$\epsilon(\mathrm{W}) = 10^7 \cdot v(\mathrm{m/s}) B^2(\mathrm{T}) \sin^4(\theta/2) \cdot l_0^2(\mathrm{m}), \tag{2.3}$$

with v being the upstream solar wind speed. Note that in *Perreault and Akasofu* [1978] the epsilon parameter was divided by a factor of 4π, produc-

ing the formula

$$\epsilon(\mathrm{erg/s}) = \frac{1}{4\pi} v(\mathrm{cm/s}) B^2(\mathrm{Gauss}) \sin^4(\theta/2) \cdot l_0^2(\mathrm{cm}). \tag{2.4}$$

Including the factor $1/4\pi$, as in equation (2.4), would cause a severe discrepancy for practically all energy budget analysis. Hereafter, equation (2.3) with SI units is used in this work, including the attached papers.

The scaling factor ${l_0}^2$ is often interpreted as being the effective cross-sectional area of interaction or the fraction of the transfer area, normalized by the efficiency of the transfer. In the original works [*Akasofu* 1981; *Kan et al.* 1980], l_0 was chosen to be 7 R_E, because that way it scaled ϵ with the obtained total energy consumption rate. For the purposes of this study, we use the original scaling of the epsilon parameter. At the end of the chapter, when discussing the total energetics, some suggestions are made to scale the epsilon to account for the needs of all known magnetospheric and ionospheric sinks as evaluated in this study.

The total amount of energy available to the magnetosphere and ionosphere is estimated by integrating epsilon from the beginning of the substorm growth phase, t_b, into the end of the recovery phase, t_e,

$$W_\epsilon = \int_{t_b}^{t_e} \epsilon \; dt. \tag{2.5}$$

The time integral of epsilon is especially useful in an input-output analysis, although the determination of the beginning and the end of the events is not straightforward. For the substorms of our data set, W_ϵ varied between $0.03 \cdot 10^{15}$ J and $60 \cdot 10^{15}$ J, roughly 95% of the events having an input less than $10 \cdot 10^{15}$ J. The average input was

$$< W_\epsilon > = \frac{1}{n} \sum_S W_\epsilon \; = \; 2.9 \cdot 10^{15} \text{ J}, \tag{2.6}$$

where n is the number of substorms and the sum is over substorms (S), while the median value

$$W_{\epsilon,med} \; = \; 1.7 \cdot 10^{15} \text{ J} \tag{2.7}$$

illustrates the typical energy input for substorms of our data set. Average substorm power, when the duration of event was taken to be four hours (Paper V), was

$$P_S = \frac{W_\epsilon}{t_e - t_b} \; = \; 2 \cdot 10^{11} \text{ W}, \tag{2.8}$$

which can be compared to the threshold power for a substorm to develop. A typical threshold power, the dynamic coupling power, to the substorms is about 10^{11} W [*Akasofu* 1981]. It is interesting to compare this to the peak power of a very strong earthquake, which is about 10^9 W.

2.1.2 Other coupling functions

The epsilon parameter is not the only parameter that can be used as a coupling function between the solar wind and the magnetosphere. Many combinations of the solar wind bulk speed, the total magnetic field, and the southward component of the total magnetic field, B_s, have been considered. For example, vB, vB^2, v^2B, vB_s, vB_s^2, v^2B_s have all been used. The transverse epsilon parameter, ϵ_T, [*Vasyliunas et al.,* 1982] is formulated in SI units as

$$\epsilon_T(\mathrm{W}) = 10^7 \cdot v(\mathrm{m/s}){B_T}^2(\mathrm{T})\sin^4(\theta/2) \cdot l_0^2(\mathrm{m}), \tag{2.9}$$

where $B_T = \sqrt{(B_y)^2 + (B_z)^2}$. The transverse epsilon is integrated through the entire substorm as

$$W_{\epsilon_T} = \int_{t_b}^{t_e} \epsilon_T \, dt. \tag{2.10}$$

In our study the integrated transverse epsilon, W_{ϵ_T}, varied between $0.004 \cdot 10^{15}$ J and $49 \cdot 10^{15}$ J, the median being about $0.8 \cdot 10^{15}$ J or roughly 50% of the total epsilon. The reason for only using the transverse component is that the Poynting flux is always perpendicular to the solar wind speed or roughly perpendicular to the GSM X-coordinate.

When the solar wind and the magnetospheric disturbances are very intense, as is the case during superstorms ($Dst <$ –240nT) [*MacMahon and Gonzalez,* 1997], the transfer function between the solar wind and the magnetosphere changes to such an extent that the pressure changes in the solar wind need to be taken into account. A ram-pressure-corrected version of Akasofu's epsilon parameter, ϵ^*, introduced by *Mac-Mahon and Gonzalez* [1997], is

$$\epsilon^* = (\frac{R_{CF}}{l_0})^2 \, \epsilon, \tag{2.11}$$

where

$$R_{CF} = (\frac{B_0^2}{\mu_0 \rho v^2})^{1/6} \, R_E. \tag{2.12}$$

Here R_{CF} is the Chapman-Ferraro radius, B_0 is the geomagnetic field at the equator and ρ is the solar wind density. *Mac-Mahon and Gonzalez* [1997] considered four very intense magnetic storms with pressure corrected Dst, denoted Dst^*, being –247 nT, –311 nT, –325 nT and –298 nT. Dst^* is typically about ten nanoteslas more negative than the original Dst [*Turner et al.,* 2001]. The ram pressure correction of ϵ is important when dealing with very intense geomagnetic events, which is, however, not the case in our study: Typically, the storms in 1997 and 1999 were around –100 nT, except for one, which was –231 nT (October 22-29, 1999). There were only two stormtime events where the epsilon pressure correction would have been needed. Therefore, we have used uncorrected Akasofu's epsilon parameter, ϵ, for computing the energy input for all events in our statistics.

2.2 Ionospheric dissipation

The most important modes of energy dissipation from the magnetosphere to the ionosphere are Ohmic Joule heating (JH) and electron precipitation (ep). All other ionospheric energy sinks, e.g., upward ion acceleration and auroral kilometric radiation are much weaker, and thus the total ionospheric energy dissipation is approximated here as $W_{ionosphere} = W_{JH} + W_{ep}$. The different ionospheric dissipation channels are not totally independent of each other. For example the electron precipitation affects the ionospheric energy deposition indirectly through Joule heating by increasing the ionospheric Pedersen conductance [*Østgaard et al.,* 2002]. However, Joule heating and electron precipitation are physically different processes and thus cannot be estimated with a single parameter.

2.2.1 Joule heating

The frictional Joule heating is caused by the ionospheric currents which heat the atmosphere at the height of around 100 km. Charged particles drift relative to each other and to the neutral particles under the action of an imposed electric field. Collisions between species limit the drift velocities and convert part of the drift energy into thermal energy. Above 125 km the electrons and ions drift at the same $\mathbf{E} \times \mathbf{B}$ speed and thus do not produce currents. Below 75 km the electron and the ion densities are too low to produce significant currents.

The Joule heating rate can be given as

$$Q_{JH} \;=\; \int_{V_{JH}} \mathbf{j} \cdot \mathbf{E}\; dX\, dY\, dZ, \tag{2.13}$$

where j is the current density in A/m^2, E the electric field in V/m and V_{JH} the volume where the collisions causing Joule heating occur. The Joule heating rate is thus proportional to the currents flowing parallel to the electric field. When it is taken into account that at high latitudes the electric field is nearly horizontal and thus almost height-independent, it is possible to introduce the Joule heating in its height-integrated form

$$Q_{JH} \;=\; \int_{A_{JH}} \mathbf{J} \cdot \mathbf{E}\; dX\, dY, \tag{2.14}$$

where J is the height-integrated current in A/m and A_{JH} the area where the collision causing Joule heating occurs. Substituting the height-integrated Ohm's law which gives currents perpendicular to the electric field, $J \;=\; \Sigma_P\, E$, to equation (2.14), Joule heating can be given as

$$Q_{JH} \;=\; \int_{A_{JH}} \Sigma_P\; E^2\; dX\, dY. \tag{2.15}$$

where the height-integrated Pedersen conductivity $\Sigma_P \;=\; \int \sigma_p dZ$.

Because ionospheric conductivities and electric fields are seldom measured at the same time over large regions, proxy formulas determining the Joule dissipation are needed. *Kamide and Richmond* [1984] constructed a model for estimating the instantaneous distributions of the ionospheric currents from ground magnetic records. To solve the problem of missing instantaneous distributions of the height-integrated quantities over the entire polar region, *Ahn et al.* [1983] devised a method of estimating Σ_P as a function of the north-south component of the horizontal magnetic disturbance, ΔH, together with an appropriate latitudinal Gaussian weighting function. With the help of the conductivity model and the empirical method, *Ahn et al.* [1983] formulated an empirical conversion formula

$$P_{JH}(\mathrm{W}) \;=\; 3 \cdot 10^8\ \mathrm{AL(nT)}, \tag{2.16}$$

where the given power is computed for the entire northern hemisphere. Instead of using hourly averages, as was done by *Ahn et al.* [1983], *Baumjohann and Kamide* [1984] used 5-min averages of the electrojet indices. Their results were consistent with those of *Ahn et al.* [1983].

Our method of converting ground magnetic measurements of the IMAGE magnetometer chain into energy dissipated by Joule heating during individual substorms includes the following steps:

(1) The IL index is constructed from the IMAGE magnetic observations (see section 1.3).

(2) The IL index is converted into the power of the northern hemisphere Joule heating $P_{JH} = 3 \cdot 10^8\, IL$ following Ahn's empirical conversion.

(3) The northern hemisphere Joule dissipation for a single event, $W_{JH,north}$, is computed by integrating the IL index from the beginning of the substorm, t_b, into the end of the event, t_e, as

$$W_{JH,north} = \int_{t_b}^{t_e} P_{JH}\, dt. \tag{2.17}$$

(4) Due to a lack of observations in the southern hemisphere the global Joule heating is approximated by doubling $W_{JH,north}$ in the following discussion.

The two-hemisphere Joule heating for substorms in our database was on average (Paper V)

$$< W_{JH} > = 2 \cdot \frac{1}{n} \sum_S W_{JH,north} = 1.3 \cdot 10^{15} \text{ J}. \tag{2.18}$$

The median for all events was

$$W_{JH,med} = 0.9 \cdot 10^{15} \text{ J}. \tag{2.19}$$

About 97% of the events had $W_{JH,med}$ less than $5 \cdot 10^{15}$ J, the highest one being $8 \cdot 10^{15}$ J. The fraction of Joule heating of the total energy input was examined by computing $(W_{JH}/W_\epsilon)_{med} \cdot 100\%$. The two-hemisphere Joule heating accounted for approximately 60% of the solar wind energy input.

2.2.2 Auroral electron precipitation

Auroral ovals are oval-shaped regions around both magnetic poles of the Earth, where active aurorae and strong geomagnetic disturbances are observed. Energy dissipation via electrons is known to be about ten times larger than the energy carried by ions [*Hardy et al.* 1989]. Three methods of estimating the electron precipitation are presented here. The first one, formulated by *Ahn et al.* [1983], is based on the Chatanika radar measurements, the second on the Explorer C and D satellite measurements [*Spiro*

et al., 1982] and the most recent one on POLAR satellite X-ray imaging [*Østgaard et al.,* 2002].

Ahn et al. [1983] present an empirical relationship converting westward electrojet index into the power of the hemispheric electron precipitation

$$P_{ep,north}(\mathrm{W}) \;=\; 0.8 \cdot 10^8\,\mathrm{AL(nT)}. \tag{2.20}$$

The result was obtained by first deriving the relationship between the height-integrated Hall conductivity (Σ_H) and auroral electron precipitation. After that *Ahn et al.* [1983] deduced a relation between Σ_H and the north-south component (ΔH) of the magnetic disturbance field.

Equation (2.20) was applied to the *IL* index. The power of electron precipitation was integrated from the start into the end of each substorm to get the energy of hemispheric electron precipitation, which was further doubled to present the global dissipation

$$W_{ep}(\mathrm{J}) \;=\; 2 \cdot \int_{\mathrm{t_b}}^{\mathrm{t_e}} P_{ep,north}(\mathrm{W})\; dt. \tag{2.21}$$

The median electron precipitation for both hemispheres, $W_{ep,med}$, was $0.27{\cdot}10^{15}$ J, which is about 30% of the typical two-hemisphere Joule dissipation.

Spiro et al. [1982] suggest that the two-hemisphere power of the electron precipitation into the auroral zone, P_{ep}, is a function of the *AE* index

$$P_{ep}(\mathrm{W}) \;=\; (1.75(\mathrm{AE}/100\mathrm{nT}) + 1.6) \cdot 10^{10}. \tag{2.22}$$

When this formula is used, the energy dissipated via electron precipitation for both hemispheres during substorms is about twice the estimate obtained from the formula (2.21) for both hemispheres.

The first global two-dimensional instrument measuring the X-ray emission was the Polar Ionospheric X-ray Imaging Experiment (PIXIE). *Østgaard et al.* [2002] used PIXIE together with the UltraViolet Imager (UVI) to derive 5-min averaged hemispherically-integrated electron energy distributions from 10 eV to 100 keV. Their data set included seven isolated substorms and the result was that the AL index could be converted into the power of the electron precipitation by

$$P_{ep}(\mathrm{W}) \;=\; (4.4\,\mathrm{AL}^{1/2} - 7.6) \cdot 10^9. \tag{2.23}$$

It is concluded on the basis of studies of *Ahn et al.* [1983], *Spiro et al.* [1982] and *Østgaard et al.* [2002] that the average two-hemisphere electron precipitation is not lower than $0.27{\cdot}10^{15}$ J, but most probably two or even four

times larger than that. If we compute the electron precipitation for average substorm event (lasting four hours, average intensity being 117 nT) the equation (2.22) gives $0.52{\cdot}10^{15}$ J whereas the equation (2.23) gives $1.15{\cdot}10^{15}$ J. Thus, the estimates based on the Spiro conversion are about two times, and Østgaard's estimates about four time the estimates given by Ahn's formula 2.21. However, results based on equations (2.21), (2.22) and (2.23) can not be directly compared, because equation (2.21) and (2.23) use AL index whereas equation (2.22) use AE index. For energy budget purposes we select $0.6{\cdot}10^{15}$ J as an estimate of typical electron precipitation energy, which is about two thirds of the two-hemisphere Joule dissipation.

2.3 Magnetospheric dissipation

The dominant magnetospheric energy sinks are ring current injections, plasmoid formation and plasma sheet heating. The ring current (RC) is a quite well studied and well-known energy sink [*Akasofu* 1981; *Hamilton et al.,* 1988], although estimates of the role of the RC in the storm and substorm energy budgets have considerable changed in recent years [*Lu et al.,* 1998; *Turner et al.,* 2001]. In the early 1980's, the RC was thought to cover about 90% of the total energy dissipation. Since then the role of other sinks have become increasingly important. Extensive studies of plasmoid energetics were conducted in the 1990's [*Kamide and Baumjohann,* 1993; *Ieda et al.,* 1998], and the energy carried away by plasmoids was found to be comparable to dissipation through other channels. In this thesis the magnetospheric dissipation is computed as a sum of ring current and plasmoid dissipation, which includes plasma sheet heating.

2.3.1 Ring current

The ring current is an equatorial westward current flowing around the Earth at altitudes 3 to 8 R_E. It results from the differential gradient, curvature, and magnetization drifts of electrons and protons in the near-Earth region. The intensity of the ring current is parameterized by the Dst index [*Sugiura and Henricks,* 1967; *Sugiura and Kamei,* 1991]. The standard method of estimating the energy carried by the ring current is

$$W_{RC} \;=\; -4 \cdot 10^{13}\left(\frac{\partial Dst}{\partial t} + \frac{Dst}{\tau}\right), \tag{2.24}$$

where τ is the ring current decay rate in seconds [*Akasofu,* 1981]. Akasofu assumed τ to be constant over the different geomagnetic conditions and he

further concluded that the main contribution to the total energy dissipation comes from the ring current energy injection rate.

At times when the solar wind pressure is high, the Dst is corrected by

$$Dst^*[\mathrm{nT}] \;=\; Dst[\mathrm{nT}] - 7.26 \cdot p[\mathrm{nPa}]^{1/2} + 11[\mathrm{nT}], \qquad (2.25)$$

where p is the solar wind dynamic pressure [*Burton et al,* 1975; *O'Brien and McPherron,* 2000]. Pressure correction is needed because variations in the solar wind pressure modulate currents flowing at the dayside magnetopause and lead to a compression of the magnetosphere, which in turn cause an increase in the Dst index. By studying seven isolated substorms, the ring current was deduced to account for 6 to 26% of the total dissipation [*Østgaard and Tanskanen,* Energetics of isolated and stormtime substorms, submitted]. These results are rather consistent with the result of *Knipp et al.* [1998] who found the ring current covering 17% of the dissipation during a magnetic storm that lasted 10 days.

O'Brien and McPherron [2000] recently argued that instead of τ being constant or varying with Dst [*Zwickl et al.* 1987], it depends on vB_s as

$$\tau(hours) \;=\; 2.40\, e^{\left(\frac{9.74}{4.69+vB_s}\right)}. \qquad (2.26)$$

In a recent paper by *Turner et al.* [2001], relations (2.24) and (2.26) were used to show that the ring current only accounts for 10%–15% of the total storm energy budget. From $W_{\epsilon,med}$ this would give $(0.17\text{–}0.26)\cdot 10^{15}$ J. Actually, this method is not suitable for measuring the ring current share of the substorm energy budget exactly: equation (2.24) is formulated to estimate the total energy dissipation to the ring current during an entire storm period, and not during a single substorm, whether occurring isolated or during a storm period. By combining the cited results we estimate that the fraction of the ring current in substorm energetics is about one third of the Joule dissipation typically ($0.3 \cdot 10^{15}$ J).

2.3.2 Plasmoids

Plasmoids are thought to be major constituents of magnetic substorms [*Kamide and Baumjohann,* 1993; *Ieda et al.,* 1998]. When reconnection begins in the tail on initially closed magnetic field lines, magnetic bubbles, called plasmoids, form and are ejected tailward. In early works [*Hones et al.,* 1976; *Hones et al.,* 1984; *Scholer et al.,* 1984a, 1984b], plasmoids were defined as topologically disconnected loop structures traveling tailward at high speeds. Later, it was demonstrated that most of these plasmoids have

helical magnetic field structures, and are thus "flux ropes" [*Hughes and Sibeck,* 1987]. Today the term plasmoid is used for both types of structures. In the magnetotail lobes, the plasmoids have been shown to produce strong "traveling compression regions" (TCRs) as they move tailward through the distant tail [*Slavin et al.,* 1984; *Slavin,* 1998].

Ieda et al. [1998] identified 824 plasmoid events from the Geotail data set. The duration of the events was typically from one to two minutes. *Ieda et al.* [1998] defined a plasmoid as being a structure with a rotating magnetic field and enhanced total pressure. They scanned visually the tail magnetic field data and identified the events from (1) the total pressure which needed to be higher inside the plasmoid than the background pressure, (2) the bipolar signatures of B_z, and (3) the plasma flow velocities which need to exceed 200 km/s in the tailward direction. Earthward moving plasmoids were excluded.

The energy transported by a plasmoid through a unit cross section of the magnetotail is typically $5 \cdot 10^{11}$ J/R$_E^2$. This was computed by *Ieda et al.* [1998] as an average of the sum of thermal ($(5/2)P_iV_x$), kinetic ($(1/2)\rho V^2 V_x$), and electromagnetic ($(\mathbf{E} \times \mathbf{B})/\mu_0$) energy flux components. They estimated plasmoid dimensions to be $L_x = 10\ R_E$, $L_y = 40\ R_E$, and $L_z = 10\ R_E$, which gives $0.16 \cdot 10^{15}$ J for each plasmoid when the form of the plasmoid is assumed to be cylindrical. *Slavin et al.* [1993] concluded that on average 1.8 plasmoids are ejected during each substorm. In addition to the energy carried "inside the plasmoid", the post-plasmoid plasma-sheet has a significant energy contribution to substorms. The contribution of each post-plasmoid plasma-sheet may be as high as $0.6 \cdot 10^{15}$ J [*Ieda et al.,* 1998]. Therefore, the total energy carried by the tailward fast flow is estimated to be

$$W_{plasmoid,estimate} \approx 0.9 \cdot 10^{15} \text{ J}, \tag{2.27}$$

which is of the same magnitude as Joule heating dissipation.

2.4 Total substorm energy budget

2.4.1 Substorm energy budget: July 8, 1997

A substorm that occurred on July 8, 1997, during which energy dissipation through all four main dissipation channels could be reasonably well estimated is discussed in detail in this subsection. The substorm onset at 2221 UT (0051 MLT) was observed at stations between 67.37° (SOD) and 78.20° (BJN). The event was a truly isolated substorm, *Dst* ranging between –5 and –14 nT during the event, the previous storm period having

taken place several weeks earlier. This particular event was followed by several isolated substorms early in the following morning, which unfortunately were out of the local night sector of the IMAGE chain.

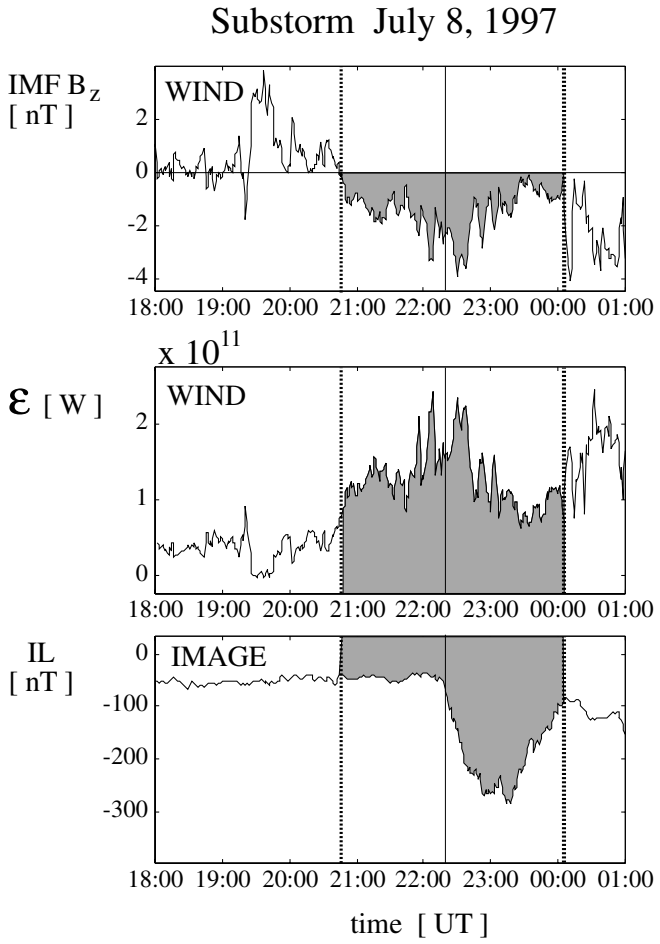

Figure 2.2: Sample event, July 8, 1997. Substorm is marked with shading.

The WIND spacecraft measured the solar wind parameters, of which $IMF\ B_z$, computed ϵ, and IL index are shown in figure 2.2. The two panels in figure 2.3 include the tail total field measured by the IMP 8 spacecraft, and the Dst index. The beginning of the event, marked by the dashed line, is determined from the B_z southward turning, and the endtime (second dashed line) is determined from the IL index recovery. The beginning of the growth phase and substorm onset times was quite clear, whereas the

ending time is less evident. This particular event was followed by another larger substorm which continued until the following morning, and thus the end time is selected at the onset of the next activation. In the light of the analysis of the separate magnetometer measurements it is clear that the first substorm returned back to quiet level, before the subsequent expansion began. IMP 8 observed a TCR slightly before 2200 UT (0030 MLT), which was identified from the tail total field and from the tail field B_Z component.

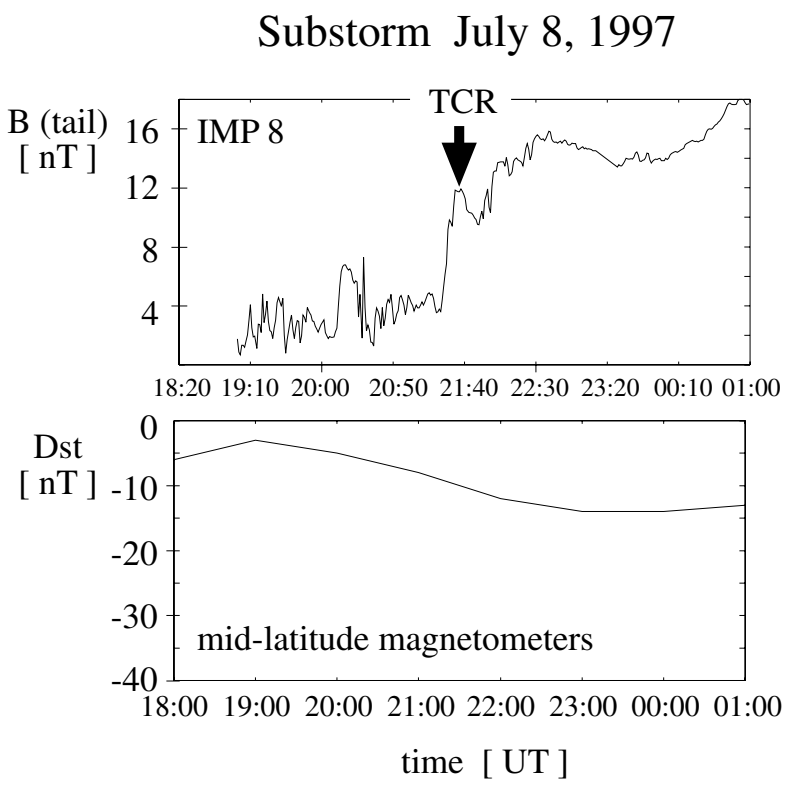

Figure 2.3: Sample event, July 8, 1997. Tail total magnetic field, measured with IMP 8 spacecraft, is shown in an upper panel and Dst index, measured with mid-latitude magnetometers, in lowel panel.

The following integrated energy parameters are given in figure 2.4: W_ϵ, W_{JH} and W_{ep}. The epsilon input was $1.7 \cdot 15$ J of which $0.92 \cdot 10^{15}$ J was dissipated by the Joule heating and about $0.61 \cdot 10^{15}$ J by electron precipitation which was computed using equation (2.21). The ring current portion is rather small because of the near-zero Dst and because of small time derivatives of the Dst. Thus, the energy dissipating to the ring current can be

excluded from the total budget. After the ionospheric dissipation through Joule heating and electron precipitation the remaining energy is $0.17 \cdot 10^{15}$ J where ϵ is used as an input estimator. This is not enough for one plasmoid and smaller dissipation channels. Thus, there seems to be an imbalance between the energy input estimate (ϵ) and the various estimates for ionospheric and magnetospheric energy dissipation. The imbalance between the input and the output can be solved by rescaling the l_0 in ϵ-parameter.

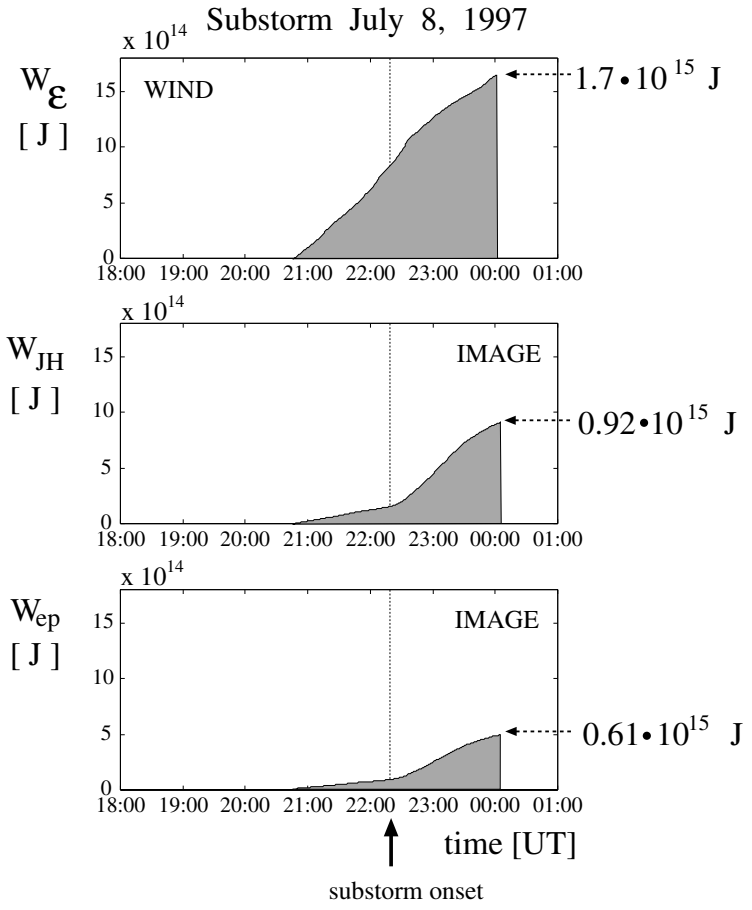

Figure 2.4: Sample event, July 8, 1997. Energy integrals for energy input, Joule dissipation and electron precipitation.

2.4.2 Statistical results

The solar wind energy reaching the Earth's magnetosphere during a typical substorm in our data set was

$$W_{IN} \approx W_{\epsilon,med} = 1.7 \cdot 10^{15} \text{ J} \tag{2.28}$$

and the total magnetospheric dissipation was

$$\begin{aligned} W_{OUT} &\approx W_{JH,med} + W_{ep,est} + W_{plasmoid,est} + W_{RC,est} \\ &\approx (0.9 + 0.6 + 0.9 + 0.3) \cdot 10^{15} \text{ J}, \\ &= 2.7 \cdot 10^{15} \text{ J}, \end{aligned} \tag{2.29}$$

where Joule heating is computed as a median, and energies dissipated into other sinks are estimated as described earlier in this section. In addition to the four included energy sinks, there are several smaller dissipation channels: ion precipitation, upward acceleration of ions, and auroral kilometric radiation. For example, ion precipitation consumes about $W_{ip} = 0.03 \cdot 10^{15}$ J [*Hardy et al.,* 1989]. It is therefore quite obvious that the energy input parameter underestimates the magnetospheric energy input. This was actually anticipated, because at the time when the coupling function was formulated in the 1980's, only dissipation into the ring current, Joule heating, and auroral precipitation was taken into account. Now that the magnitude of the energy carried by the plasmoid and post-PPS have been estimated, the epsilon parameter needs to be rescaled.

2.5 Discussion

Twenty years after the introduction of the epsilon parameter, it is still a valid tool for estimating the magnetospheric energy input. However, the original definition of the scaling factor l_0 seems to be somewhat too small. The main reasons for this are that plasmoids and plasma sheet heating were not taken into account in the original energy budget analysis, and that new estimates for Joule dissipation and auroral precipitation have increased their role. Assuming that the estimates given by *Østgaard et al.* [2002] for the precipitation energy and those given by *Ieda et al.* [1998] for the plasmoid and post-plasmoid plasma sheet are correct, the average total energy input, W_{OUT}, sums up to $3{\cdot}10^{15}$ J, which is larger than the typical energy input, $W_\epsilon \approx 2{\cdot}10^{15}$ J. We suggest that a factor of 1.5 for rescaling the l_0^2 parameter is adequate and that it is likely that no more than a factor of 2 would be needed.

A rescaling of the energy input is also suggested by *Østgaard and Tanskanen* [Energetics of isolated and stormtime substorms, submitted] who studied the energetics of seven isolated substorms without including the tail dissipation in the total output. They also concluded that for some events ϵ does not provide enough energy for the magnetosphere-ionosphere system. Comprehensive AMIE studies on storm energetics also indicate that the integral of ϵ remained below the total energy consumption [*Knipp et al.,* 1998; *Lu et al.,* 1998; *Turner et al.,* 2001]. Further complications may arise, as the scaling parameter l_0 does not need to be the same for every event. The input efficiency may also depend on the solar wind dynamic pressure [*Shue et al.,* 1997, 1998].

Most of the solar wind energy is dissipated into the ionosphere during magnetospheric substorms. Statistical results from 839 substorms in 1997 and 1999 show that Joule dissipation consumes about 60% of the total ϵ input and electron precipitation about half of that. The remaining energy is consumed by plasmoids and plasma sheet heating together with a small portion dissipated by the ring current. This result is confirmed by *Østgaard and Tanskanen* [Energetics of isolated and stormtime substorms, submitted] who found that the energy transferred from the solar wind to the magnetosphere-ionosphere system is distributed such that on average 15% goes to the ring current, 56% to Joule heating, and 29% to auroral precipitation.

Chapter 3

Properties of substorms

Although all substorms are different, it is still possible to calculate average properties characterizing a typical substorm. The events in our data set were described with the following measures: duration, frequency, onset latitude, onset time, maximum intensity, and substorm size. The entire substorm process is examined by using two distinct processes in the substorm evolution: directly driven (DD) activity and loading-unloading process, which is here discussed in the context of the near-Earth neutral-line (NENL) model.

3.1 Duration, frequency, latitude, and onset time

We define the duration of the substorm (Δt) as the time period between the beginning of the growth phase (t_b), and the end of the recovery phase (t_e). The average duration for all events in our database was 3 hours 50 minutes of which the growth phase took on average about 60 minutes. Figure 3.1 shows the histogram on substorm durations binned by every 30 minutes. The duration of the expansion and recovery phases, 2h 50min, may be slightly underestimated, due to the limitations of the local IMAGE magnetometer network to record activity after 0200 UT. However, only a limited number of events continued beyond 0200 UT. The substorm frequency, f, was computed by dividing the total number of events, n, by the total period of time, T,

$$f \;=\; \frac{n}{T} \;=\; \frac{839}{7669\ \mathrm{h}} \;\approx\; 0.11\,\mathrm{h}^{-1}. \tag{3.1}$$

At times there were several substorms in one day, but at other times, during the most quiet periods, there were several days without substorm activity in the IMAGE sector.

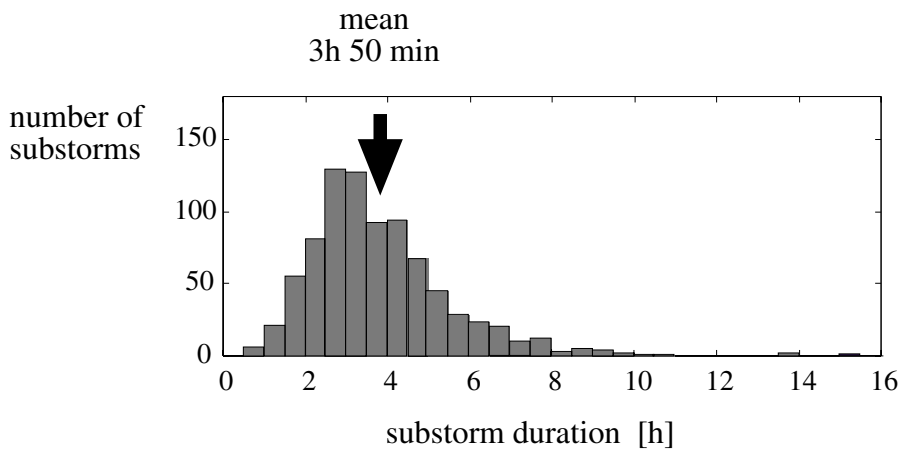

Figure 3.1: Distribution of substorm length. Histogram is binned in every 30 minutes.

Figure 4a in Paper V summarizes the number of substorms in five different latitudinal zones. The zones were selected from south to north in geographical coordinates as follows: (1) south of 65°, (2) 65° – 69°, (3) 69° – 73°, (4) 73° – 76°, and (5) north of 76°. The corresponding IMAGE magnetometer array stations are (1) UPS, NUR, HAN, OUJ, LYC, (2) PEL, SOD, KIR, LOZ, MUO, ABK, (3) KIL, AND, MAS, TRO, KEV, SOR, (4) BJN, and (5) HOP, HOR, LYR, and NAL (See Appendix A). Substorms were categorized in the latitude bins according to the station where the maximum deviation of the X component was recorded. The majority of the substorms, over 40%, were located in the central zone (bin 3) above the northern part of Fennoscandia. The total numbers of events in all five zones from south to north were: 18, 77, 348, 199, and 197. Nine events out of ten had the maximum |IL| at a latitude higher than the standard AE station Abisko. Thus, longitudinal chains of magnetometers, in addition to the standard AE network, have special value in studies of magnetospheric substorms. The typical onset time, t_o, computed as a mean value, was 2250 MLT. The onset times had a nearly Gaussian distribution over the time period 16 – 02 UT (1830 – 0530 MLT).

3.2 Intensity and size

In this thesis the substorm intensity, I, is defined as max(|IL|) determined by the largest deviation of the north (X) component of the IMAGE chain westward electrojet index. In the event identification, one of our selection criteria was that subtorms had to exceed 100 nT in intensity. The threshold of –100 nT is a random choice, as there is no unique minimum level of electrojet activity which would distinguish substorms from other types of disturbances. The typical intensity was computed as a mean for all substorms, being about 400 nT for the entire statistics. Two-year averages for substorm intensities were computed separately in each latitudinal zone. The averages from the south to the north were 727 nT, 639 nT, 407 nT, 313 nT, and 363 nT. The most intense substorms took place at the lowest latitudinal bin, south of 65°. However, these were quite rare events occurring as south as in Oulujärvi (OUJ), Hankasalmi (HAN) and Nurmijärvi (NUR).

There are several methods by which the size of substorms can be estimated, one being the substorm intensity discussed above. Another method is to integrate the Joule heating over the substorm, W_{JH}, and use that as a measure of substorm size. The main problem with this method is the uncertainty in the determination of the exact time of the beginning and the end of the substorms, as well as in the computation of the JH rate from the electrojet indices. When this definition was used the smallest substorm in our database is $0.06 \cdot 10^{15}$ J and the largest one $8 \cdot 10^{15}$ J. Both events took place during non-storm times, showing a positive Dst during the smallest event and a slightly negative Dst (between –17 nT and –24 nT) during the largest event. Table 3.2 summarizes parameters characterizing substorms in our data set.

Δt mean	f mean [1/h]	t_o mean [MLT]	I mean [nT]	W_{JH} mean [10^{15} J]	W_{JH} median [10^{15} J]	$\frac{W_{JH}}{W_\epsilon}$ mean [%]	$\frac{W_{JH}}{W_\epsilon}$ median [%]
3h 50 min	1/9	22:50	400	1.3	0.9	77	60

Table 3.2 Entire database, 839 substorms, characterized by the following parameters: duration (Δt), frequency (f), time of onset (t_o), intensity (I), size (W_{JH}) and ratio W_{JH}/W_ϵ. Both means and medians are given for the sizes and ratios.

3.3 External and internal contributions to the IL index

Magnetic variations observed on the Earth's surface and studied with the IL index are caused by sources both external and internal to the Earth. External variations arise from the currents in the ionosphere and magnetosphere, whereas the internal variations are caused by currents induced in the solid Earth. To examine the external and internal contributions to the IL index, 77 relatively isolated substorms were selected. As additional criteria for event selection for our large statistics, we required data from at least at 10 stations along the NUR-NAL chain (NUR-HAN-OUJ-PEL-MUO-MAS-SOR-BJN-HOR-LYR-NAL). The internal, X_{int}, and external, X_{ext}, contributions at each station were derived by using the Siebert-Kertz formulation [*Weaver,* 1964] separately for each substorm. The Siebert-Kertz separation integrals are given in equation (4) of Paper IV. The IL_{ext} and IL_{int} were constructed by computing the envelope from X_{int} and X_{ext} of the individual stations in the same manner as it was done for the IL index.

The superposed epoch curves with IL, IL_{ext} and IL_{int} were formed for the 77 events. The internal contribution peaks strongly after the substorm onset and then decays over a time period of about 30 min. In figure 3.2 the ratio IL_{int}/IL_{tot} is shown as a function of the substorm phase. The results shown by this figure are that the internal component is about 40% of the total field variation around the substorm onset time and that the average portion of the internal component during the entire substorm is about 20%. Furthermore, the internal contribution to the total magnetic field is between 30% and 40% during the expansion phase and between 10% and 30% during the substorm recovery.

Superposed epoch curves for the events occurring in different local time sectors were also computed. The events were divided into three categories according to the onset times: (1) evening sector events with onset times before 1900 UT (2130 MLT), (2) midnight events with onsets between 1900 UT and 2200 UT ($2130 < \text{MLT} < 0030$), and (3) morning sector events occurring after 2200 UT (MLT > 0030). The number of events in the three time sectors were 38, 32 and 7, respectively. Induction effects were strongest for the evening sector events, where the effect on the IL index time derivative was largest. In the morning sector the induction effects were small, and their contribution to the index does not actually maximize until after the peak of the substorm intensity. This is because the most localized and strongest currents are associated with the westward traveling surge in the evening

sector.

The latitudinal variation of the induction effects was studied by computing the average of IL_{ext}/IL_{tot} for all substorms that were categorized as belonging to one of the following nine IMAGE magnetometer stations: OUJ, PEL, MUO, MAS, SOR, BJN, HOR, LYR and NAL depending on where the maximum disturbance was recorded. The four high-latitude stations located over the Arctic Ocean above 70° show about 70% values of the ratio IL_{ext}/IL_{tot}, while the external variations amounted to 80% of the total field variations in the mainland. The larger induction in the oceanic stations, compared to the mainland stations, is caused by the better conductivity of the sea water.

The internal portion of the IL index is quite large, especially at the substorm onset, and it needs to be taken into account when using the maximum of $|IL|$ index as a measure of substorm size.

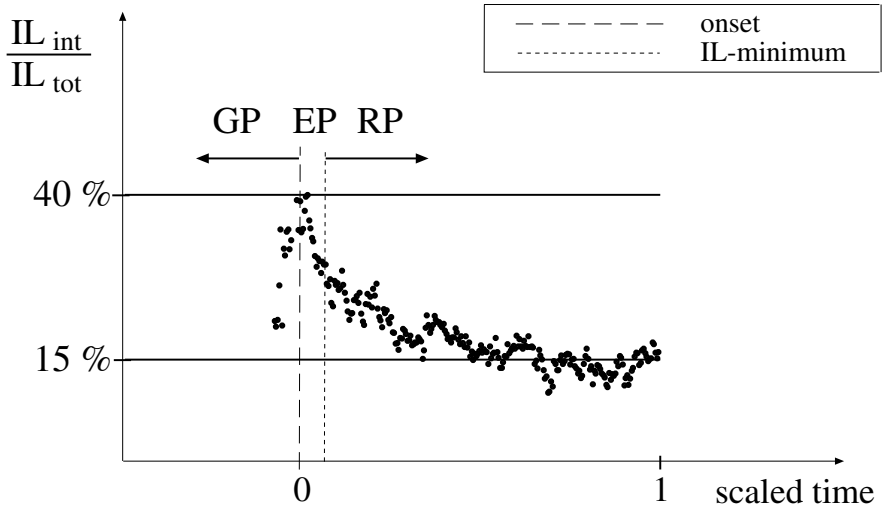

Figure 3.2: Superposed epoch curve about induction effects to IL index.

3.4 Directly driven and loading-unloading processes

The NENL model [*McPherron et al.,* 1973; *Russell and McPherron* 1973] is one of the earliest and today one of the best-developed models for the substorm dynamic cycle. In the NENL model, the substorm begins when a southward turning of the IMF activates the dayside reconnection. The dayside magnetic flux is transported tailward over the polar cap, where it is

added to the tail lobes. During this growth phase, the tail lobe field increases and the plasma sheet thins. During the late growth phase, a new neutral line forms in the near-Earth tail and a slow reconnection in the tail begins. As the plasma density decreases, the reconnection rate at the NENL increases until the process grows explosively at the expansion phase onset. The following substorm (particle injections, auroral precipitation, tail reconfiguration and plasmoids) gains power from the unloading of energy stored in the tail lobes during the growth phase.

It is a generally accepted fact that substorms consist of both directly driven and loading-unloading processes [*Baker et al.,* 1981] (see figure 3.3). The DD process [*Perreault and Akasofu,* 1978; *Akasofu* 1979, 1980, 1981] was introduced to explain the close relationship between the energy input parameter and the AL index. The DD scenario assumes that reconnection occurs at the dayside magnetosphere, opening the magnetic field lines of the polar cap to the solar wind. In addition, the scenario assumes that a solar wind dynamo drives electrical currents in the ionosphere and magnetosphere. Once the polar cap magnetic field lines are opened, the motion of the solar wind across the open field lines acts as a generator, producing a voltage that is transmitted by the field lines to the polar ionosphere. In this DD scenario most of the energy powering the ionospheric activity comes from the reconnection of newly arrived flux tubes during the expansion phase, while in the NENL model most of the energy comes from the tubes reconnected earlier.

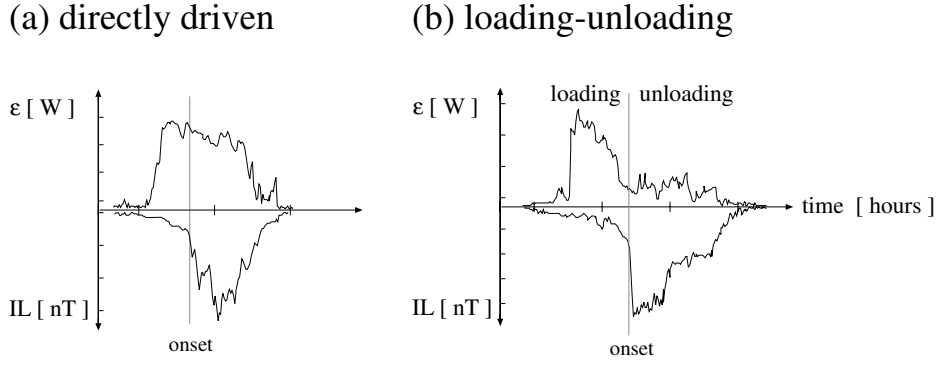

Figure 3.3: Sketches of directly driven and loading-unloading events.

By using linear prediction filters, it has been shown that isolated substorms are characterized by a bimodal response function [*Clauer et al.,* 1981; *Bargatze et al.,* 1985, 1986]. One component of this response function reacts

to the solar wind and IMF change in about 20 minutes, whereas the other peak is delayed by about an hour. The rapidly responding component is apparently the directly driven response of the ionosphere to the solar wind driving [*Akasofu,* 1981] and the delayed component represents the unloading of energy stored in the magnetotail [*Baker et al.,* 1984; *Baumjohann,* 1986]. Traditionally, it has been assumed that the substorm process mainly dissipates energy stored during the growth phase [*Baker et al.,* 1984]. This assumption will be examined in more detail below.

3.5 Energy input-Joule heat correlation

The directly driven properties of the substorm data set are examined by correlating the magnetospheric energy input, W_ϵ, with the ionospheric Joule dissipation, W_{JH}. The solar wind data are shifted to the magnetopause to make sure that the correlations are done correctly. The solar wind plasma slows down approximately by a factor of four as it crosses the bow shock near the subsolar point. However, as the subsolar distance from the shock to the magnetopause is only about 3 R_E, this effect is not taken into account here. On the basis of this assumption, the solar wind data series are shifted by using the X-distance between the data-producing spacecraft and the nose of the magnetopause, ΔX, divided by the solar-wind convection velocity averaged over the event.

The linear correlation coefficient between the total energy input and two-hemisphere Joule dissipation was computed as being 0.57 for the entire data set, 839 substorms. Significantly higher correlations were found for specific groups of substorms presented in more detail in chapter 4. When the growth phase and the expansion phase were examined separately, and the correlations were computed separately for the substorm growth phase and the expansion phase, the correlation was at its highest, 0.63, between expansion phase input and output. This indicates that the size of the substorm mainly depends on the amount of energy input during the expansion phase. The energy input and output during the growth phase correlated very poorly, which is evident in figure 3 in Paper I. That study was made for the isolated substorms in 1997 only, but the same conclusions apply to the entire data set. The energy input during the growth phase was quite similar for all events, of the order of 10^{15} J, regardless of the size of the substorm that follows. Although the growth phase input does not greatly affect the size of the substorm, it is important for the preconditioning of the magnetotail to allow the global instability to grow.

The correlation study was repeated by using the transverse epsilon parameter, W_{ϵ_T}, instead of the standard epsilon, for the events in 1997. W_{ϵ_T} was clearly lower than W_ϵ, but there was no significant difference between the correlations W_{JH}-W_ϵ and W_{JH}-W_{ϵ_T} (Paper III).

3.6 Discussion

Our two-year data set included 839 substorms with onsets between 16–02 UT, of which 352 took place in 1997 and 487 in 1999. Only events that had both the beginning and end within this time period were included into the data set. Thus, many substorms were left out from the database because the IMAGE chain would not necessarily record the strongest activity. In order to get the total number of substorms that occurred in 1997 and 1999, the number of events in the data set needed to be multiplied approximately by three. This number is consistent with the analysis done by *Borovsky et al.* [1993] who identified substorms from energetic particle injections at geostationary orbit. They found 1530 substorms at the time interval from October 1, 1982, to September 29, 1983, during a period of descending solar activity. *Kamide* [1982] analyzed substorms that took place in 1978, near sunspot maximum, using the AL index and data from certain International Magnetospheric Study (IMS) magnetometer records. They found 1360 substorms, the lower limit for substorm intensity being 200 nT. Thus, it seems that both particle injections and westward electrojets can be successfully used for substorm identification so that the results yield consistent values for yearly substorm occurrence. The yearly number of substorms is thus between 1000 and 1500, depending on the solar cycle phase. However, none of these statistical studies covered years of maximum solar activity, during which the yearly number of substorms may exceed 1500.

It was found on the basis of our data set, that isolated substorms occurred every ten hours while stormtime substorms occurred every four hours. Our method of computing the frequencies included all moments of time, regardless of the solar wind conditions, and therefore it does not provide a consistent comparison between the two classes of substorms. The data covered several long periods (several days) where no substorms occurred. If we had included only times when the solar wind conditions were favorable for substorm activity, the frequency of isolated substorms would have been much higher, even close to the frequency of stormtime substorms. *Borovsky* [1993] examined substorms that occurred under favorable solar wind conditions, i.e., that the IMF Z-component was southward for an extended

period of time. They found the average occurrence time difference from one substorm onset to another to be 5.74 hours, with a significant peak between 2 and 4 hours in the statistics. This is comparable to the duration of substorms in our statistics, which was about four hours on average, showing a broad peak between 2 and 5 hours.

The substorm intensity, measured as the minimum of the IL index, has shown to be a good parameter for measuring the substorm size, but it is in no way a perfect parameter. This is partly because the auroral electrojet indices record both external and internal variations [*Viljanen et al.,* 1995]. The internal part of the IL (and AL) is largest for the rapid time variations, such as substorm onsets, where the internal part can be as high as 40% of the IL index (Paper IV). The internal contribution decreases during the expansion and recovery phases to an average of about 15 –20% during non-disturbed times (Paper IV). Thus, the maximal negative variation of the IL index can be used as a measure of substorm size, considering that part of it is caused by induction effects.

The use of $\max(|IL|)$ as a measure of substorm size is further complicated by the fact that the internal part of the IL index also varies as a function of latitude. The stations located over the Arctic Ocean, e.g. Bear Island (BJN), show larger induction effects than the inland stations. For example, the induction effect is about 30% of the total IL index at BJN, (geor.lat. 74.50°, geogr.long. 19.20°), whereas it is about 10% at Muonio, MUO, (geogr.lat. 68.02°, geogr.long. 23.53°). Thus, when comparing maximum intensities at different latitudes, they should be corrected for the induction effects.

The size of a substorm was found to be determined by the energy input during the substorm expansion phase (Paper I, Paper V). Thus, the substorm energetics seem to be largely controlled by the directly driven processes. However, loading of energy is needed during the substorm growth phase for the preconditioning of the magnetosphere, to allow for the global instability to grow.

In some events, e.g. in the July 24, 1997 substorm [details in *Østgaard and Tanskanen et al.,* Energetics of isolated and stormtime substorms, submitted], the total dissipation was observed to be more than twice the total energy input. This inconsistency in the energetics can be partly corrected by rescaling the input parameter, but it is also possible that the energy had been stored already much earlier. This is impossible to conclude on the basis of the available data. However, it is important to note that an exact energy balance between input and output is only required over long time scales and not in individual substorm periods.

Chapter 4

Different types of substorms

The substorms in the data set were divided in four different ways: 1) isolated (IS) and stormtime substorms (SS), 2) quiet year substorms (S97) and active year substorms (S99), 3) continuous input substorms (S_{cont}) and growth phase input events (S_{GP}), and 4) substorms occurring poleward (S_{pole}) and equatorward (S_{equ}) of Abisko. Events were said to be isolated whenever there was no storm activity, as measured by the Dst index, during the event. In the present study the Dst threshold for a storm was –40 nT. The different types of substorms are compared in this chapter by using the characteristics presented in chapter 3.

4.1 Isolated and stormtime substorms

Recently, the fundamental differences between isolated and stormtime substorms have been subject to a lively debate [*Baumjohann et al.,* 1996; *Kamide et al.,* 1998; *Hsu and McPherron* 2000]. The data set used for the present thesis allows this question to be addressed, as we have 698 isolated and 141 stormtime events. The number of isolated substorms was much larger than the number of stormtime substorms, but also the total period of time was longer when $Dst > -40$ nT. The frequency of isolated substorms (f_{IS}) was computed by dividing the total number of the isolated events, n_{IS}, by the total period of time in 1997 and 1999 during which the $Dst > -40$ nT and IMAGE was in the night sector:

$$f_{IS} = \frac{n_{IS}}{T_{IS}} = \frac{698}{7106\,\mathrm{h}} \approx 0.1\,\mathrm{h}^{-1}. \quad (4.1)$$

Correspondingly, the frequency of the stormtime events was

$$f_{SS} \;=\; \frac{n_{SS}}{T_{SS}} \;=\; \frac{141}{563\,\mathrm{h}} \;\approx\; 0.25\,\mathrm{h}^{-1}, \tag{4.2}$$

where n_{SS} is the total number of the stormtime events and T_{SS} the total time during which $Dst \leq$ –40 nT and IMAGE was in the night sector. If only the favorable SW conditions were counted, the frequency of isolated substorms would be close to the frequency of stormtime substorms.

The histograms of total magnetospheric energy input, $W(\epsilon)$, and the two-hemisphere Joule dissipation, W_{JH}, are illustrated in figure 4.1, for the isolated and stormtime events. The typical value of energy input is $0.14{\cdot}10^{16}$ J for isolated substorms while it is $0.35{\cdot}10^{16}$ J for stormtime events. Both input distributions have long tails, with a total of ten events having $W(\epsilon)$ larger than $2 \cdot 10^{16}$ J. As regards the output, or Joule heating, most events occur in the lowest bin of below $0.1 \cdot 10^{16}$ J for isolated substorms, while the maximum is at $0.2 \cdot 10^{16}$ J for stormtime events. The isolated substorms are five times more numerous than the stormtime substorms, but their energy input is only half of that of the stormtime substorms. The Joule dissipation varied from values below 10^{14} J to values larger than $6 \cdot 10^{16}$ J, the median being $0.8{\cdot}10^{15}$ J for isolated and $1.8{\cdot}10^{15}$ J for stormtime events.

During the studied two-year period, the two-hemisphere Joule dissipation through isolated events was

$$\sum_{IS} W_{JH} \;=< W_{JH,IS} > \; n_{IS} \;\approx\; 7.7 \cdot 10^{17}\ \mathrm{J}, \tag{4.3}$$

and the dissipation through stormtime substorms was

$$\sum_{SS} W_{JH} \;=< W_{JH,SS} > \; n_{SS} \;\approx\; 3.4 \cdot 10^{17}\ \mathrm{J}. \tag{4.4}$$

Although single isolated substorms dissipate less energy than single stormtime substorms, on average, the yearly Joule heating through the isolated substorms is larger than the heating through the stormtime substorms. This is because isolated events are five times more numerous than the stormtime events. The Joule heating percentage of the energy input, (W_{JH}/W_{ϵ}), was computed for both isolated and stormtime events. The histograms of the ratios are plotted as a function of the number of substorms in figure 9 in Paper V. The ratio for the medians indicate that the two-hemisphere JH accounted for roughly two thirds of the input for isolated events and about fifty percent of the input for stormtime events. This indicates that the role

of Joule heating is more important, as compared to the other energy sinks, during isolated substorms than during storm periods. The most likely reason for this is the more significant role of the ring current during the storm periods.

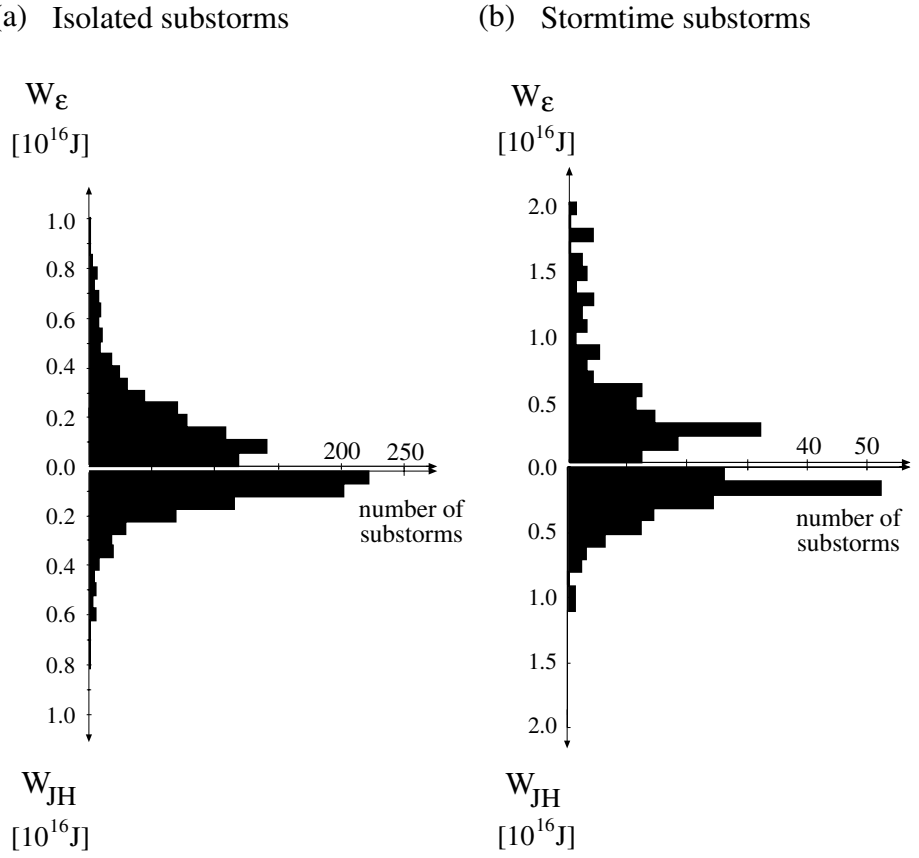

Figure 4.1: (a) Energy input, W_ϵ, and two-hemisphere Joule dissipation, W_{JH}, histograms for isolated substorms. Both histograms are binned by every $0.5 \cdot 10^{15}$ J. (b) Energy input and two-hemisphere Joule dissipation histograms, binned by every 10^{15} J, for stormtime substorms of our data set. Note that the scales are different.

The average intensity for isolated substorms was 347 nT and for stormtime substorms 665 nT. The medians were about 50 nT smaller than the means for both types of events, indicating that the intensity distributions

were not Gaussian. Furthermore, the low-intensity substorms, less intense than –400 nT, were almost totally absent from the stormtime events, but were quite numerous in the group of isolated substorms. However, the maximum intensities for both isolated and stormtime substorms were about –1700 nT.

The correlation between the energy input and the Joule dissipation for the isolated and the stormtime events were 0.71 and 0.58, respectively. In figure 8 in paper V, the regression line for the stormtime substorms has been drawn from a zero input to the maximum energy input for isolated events, $1.87 \cdot 10^{16}$ J. The reason for cutting the regression analysis at this level is that, for very large input energies, the ionospheric dissipation does not seem to grow with the energy input. By including only these events with an input less than $19 \cdot 10^{15}$ J, the correlation is improved from 0.58 to 0.65. The conclusion already made in respect of the entire database applies to both isolated and stormtime substorms separately: the correlation coefficient between the substorm expansion phase input and the expansion phase output is larger than the coefficient between the total input and the total output. This means that the duration and intensity of energy dissipation during the substorm expansion phase is not determined by the energy stored during the growth phase but rather by the energy which continues to be transferred to the magnetosphere during the expansion phase. Correlations were further improved up to 0.81, when only post-midnight substorms ($t_o > 2400$ MLT) were taken into account.

Latitudinal distribution of maximum intensities show some differences. The number of isolated substorms was much larger than the number of stormtime substorms in the three most northern latitudinal zones, at zones 3,4 and 5. At latitudes lower than 65° (geogr. lat) substorms were mainly of stormtime type.

The substorm onset times showed slight differences between isolated and stormtime events: the onset for stormtime substorms was at 2300 MLT and for isolated substorms 45 minutes earlier. Apart from this and other previously mentioned differences there were also some similarities between isolated and stormtime substorms. Isolated and stormtime events were similar in terms of duration. The average duration of isolated substorms was slightly less than 4 hours whereas duration was about 4 hours, on average, for stormtime substorms. Table 4.1 lists the key characteristics separately for stormtime and isolated substorms and figure 4.2 shows sketches of a typical isolated and stormtime substorm.

(a) Typical isolated substorm

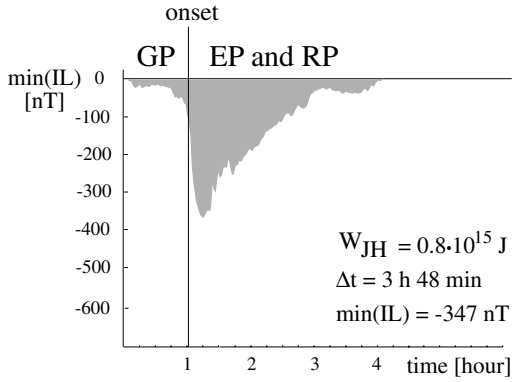

(b) Typical stormtime substorm

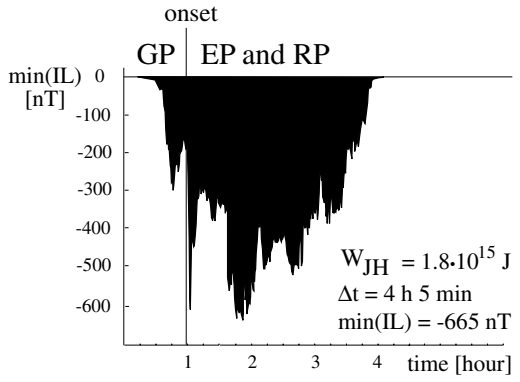

Figure 4.2: A sketch of a typical isolated and stormtime substorm.

	Δt mean	f mean [1/h]	t_o mean [MLT]	I mean [nT]	W_{JH} mean [10^{15} J]	W_{JH} median [10^{15} J]	$\frac{W_{JH}}{W_\epsilon}$ mean [%]	$\frac{W_{JH}}{W_\epsilon}$ median [%]
IS	3h 47 m	1/10	23:01	347	1.1	0.8	80	61
SS	4h 5 m	1/4	22:14	665	2.4	1.8	61	48

Table 4.1. Comparison of isolated, IS, (698 events) and stormtime, SS, (141

events) substorms in terms of the following parameters: duration (Δt), frequency (f), onset time (t_o), intensity (I), size (W_{JH}) and ratio W_{JH}/W_ϵ. Both means and medians are presented for the sizes and the ratios.

4.2 Substorms during low and high solar activity

This thesis contributes to the discussion of solar cycle effects to substorm activity through the study of substorms during low solar activity (S97) and high solar activity (S99) (Paper V). Substorms in the high-activity year account for 58% of all the events included in our database. No data were available at the end of 1999 but the statistics are extensive enough (352 + 487 substorms) to identify differences between the substorms that took place during the two phases of the solar cycle.

The yearly median of energy input for substorms during low-activity solar cycle phase was about $1.2 \cdot 10^{15}$ J and in the high-activity phase $2.1 \cdot 10^{15}$ J. The annual median of Joule heating was only slightly larger, by $0.1 \cdot 10^{15}$ J, for the more active solar cycle phase. The histograms of the ratios (W_{JH}/W_ϵ) are plotted as figure 11b in Paper V, with the medians marked with arrows. The differences in the medians of the ratios (see also table 4.2) were more than ten percent units, indicating that the role of Joule heating, and further the role of the ionosphere, in the energy budget decreases towards higher solar activity.

Another clear difference was identified in the latitudinal locations of substorm onsets (figure 4 in paper V). The object of the present study was to examine latitudinal range between 60° and 80°. A vast majority of the substorms were located to the north of Abisko (N68.35, E18.82) during both years, the most events occurring between the geographic latitudes 69° and 73°. During the more quiet year substorms very seldom occurred south of 69°, but during the more active year about fifteen percent of the events took place in the two southernmost zones, below 69°. The other characteristics (table 4.2) did not show significant differences between substorms during low and high solar activity.

It is worth mentioning that there seems to be an upper limit of W_{JH} and thus of the substorm intensity, which gets higher as the Sun becomes more active. The maximum intensity in 1997 was 1400 nT, which was the same for both isolated and stormtime events, whereas the limit was 1700 nT in 1999. However, as the results are given for two years only and can therefore not be generalized in a straightforward manner, it would be interesting, in the future, to examine the annual averages for the entire solar cycle.

	Δt mean	t_o mean [MLT]	I mean [nT]	W_{JH} mean [10^{15} J]	W_{JH} median [10^{15} J]	$\frac{W_{JH}}{W_\epsilon}$ mean [%]	$\frac{W_{JH}}{W_\epsilon}$ median [%]
S97	4h 2 min	22:56	376	1.3	0.9	77	61
S99	3h 42 min	22:51	418	1.4	1.0	67	49

Table 4.2. Comparison of substorms in 1997 (S97) and 1999 (S99) in terms of the following parameters: duration (Δt), time of onset (t_o), intensity (I), size (W_{JH}) and ratio W_{JH}/W_ϵ. Number of substorm was 698 in 1997 and 141 in 1999. Both means and medians are presented for the sizes and ratios.

4.3 Growth phase input and continuous input substorms

The events where the solar wind input terminates near the substorm onset (S_{GP}), and the events where the energy input continues throughout most of the expansion and recovery phase (S_{cont}) were also examined separately (figure 4.3). The purpose of this was to find out whether the energy input decrease near the substorm onset has effects on the substorm characteristics. It was found that the energy input affects the intensity and size of the substorm, but not to the same extent as the simultaneous storm activity (compare tables 4.1 and 4.3). In cases where the energy input continued past the substorm onset, the substorm intensity and size are larger than in cases where the input stopped near the onset. As seen in figure 4.4, the growth phase input events dissipated less energy in Joule heating than the continuous input events, when compared to events with similar maximum intensity.

It was concluded in section 3.5 that the energy input during substorm growth phase does not greatly affect the size of the substorm. That is actually true for S_{cont} events only, which constitute the majority of substorms in our data set (table 4.3). For S_{GP} events the energy input during the growth phase was 10^{15} J, while the input during the rest of the event remained at $0.5 \cdot 10^{15}$ J. For continuous input events the average energy input during the growth phase was $0.9 \cdot 10^{15}$ J and the average input during the rest of the event about $2.3 \cdot 10^{15}$ J.

(a) Continuous input substorm (b) Growth phase input substorm

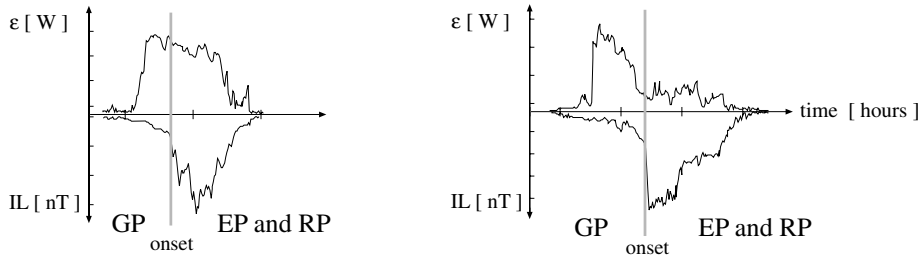

Figure 4.3: Sketches about continuous input and growth phase input events.

	Δt mean	t_o mean [MLT]	I mean [nT]	W_{JH} mean [10^{15} J]	W_{JH} median [10^{15} J]	$\frac{W_{JH}}{W_\epsilon}$ mean [%]	$\frac{W_{JH}}{W_\epsilon}$ median [%]
S_{GP}	3h 13 min	22:49	328	0.8	0.6	74	55
S_{cont}	4h	22:54	419	1.5	1.0	70	57

Table 4.3. Comparison of continuous input substorms (S_{cont}) and growth phase input substorms (S_{GP}) in terms of the following parameters: duration (Δt), time of onset (t_o), intensity (I), size (W_{JH}) and ratio W_{JH}/W_ϵ. Number of S_{GP} substorm was 171 and number of S_{cont} substorms 668. Both means and medians are presented for the sizes and ratios.

4.4 Poleward and equatorward substorms

Substorms can also be classified according to the onset latitudes. In the present study the events were divided into those located north of Abisko (S_{pole}) and those located equatorward of Abisko (S_{equ}). This is the first statistical study in which the substorms are separated in the terms of latitudes, and the preliminary results need to be analyzed further. The standard characteristics are evaluated in table 4.4.

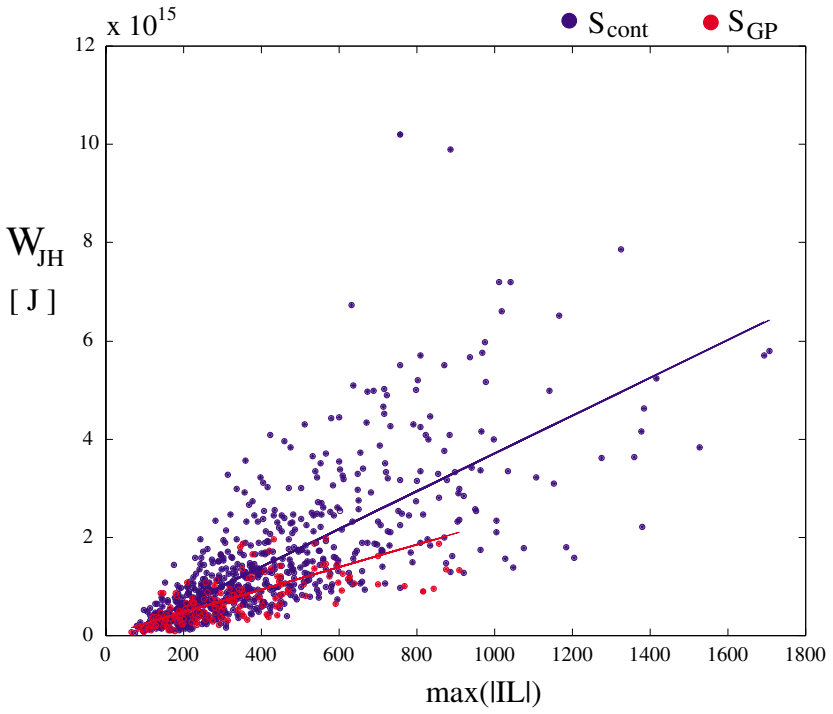

Figure 4.4: Substorm intensity vs. substorm size (W_{JH}), separately for continuous input and growth phase input substorms.

	Δt mean	t_o mean [MLT]	I mean [nT]	W_{JH} mean [10^{15} J]	W_{JH} median [10^{15} J]	$\frac{W_{JH}}{W_\epsilon}$ mean [%]	$\frac{W_{JH}}{W_\epsilon}$ median [%]
S_{pole}	3h 24 min	21:51	338	0.8	0.9	70	52
S_{equ}	4h 13 min	23:59	456	1.8	1.0	74	60

Table 4.4. Comparison of poleward (S_{pole}) and equatorward substorms (S_{equ}) in terms of the following parameters: number (n), duration (Δt), time of onset (t_o), intensity (I), size (W_{JH}) and ratio W_{JH}/W_ϵ. Both means and medians are presented for size and ratio.

The most striking difference is identified in the onset times, the average onset of S_{equ} being near local midnight, which is consistent with earlier studies [*Akasofu* 1964; *Caan et al.,* 1978]. The average onset for the poleward events was two hours earlier at 2151 MLT. All the other parameters were as expected; equatorward events lasting longer, being slightly more numerous and more intense. When the induction effects to the substorm intensity are taken into account, as was suggested in chapter 3.3, then the average intensity of poleward substorms will be 237 nT and the average intensity of equatorward substorm about 410 nT.

4.5 Discussion

Only a fraction of substorms can be categorized as typical substorms. Isolated and stormtime substorms were studied by *Baumjohann et al.* [1996] who suggested that these two classes of substorms are produced by different mechanisms: isolated substorms by current sheet disruption [*Lui et al.,* 1988] and stormtime substorms by near-Earth reconnection [*McPherron et al.,* 1973, *Hones et al.,* 1984]. *Baumjohann et al.* [1996] results showed that isolated substorms did not increase and decrease the tail lobe field, whereas stormtime substorms exhibited the typical substorm tail features: loading of energy during the growth phase, dipolarization at the substorm onset and unloading after the onset. *Hsu and McPherron* [2000] argued that both classes of substorms are caused by the same mechanism. Even so, they found some differences between the two classes of substorms, in respect of absolute values and changes of magnitude. The stormtime substorms were larger than the isolated ones in their statistics. This is consistent with our results showing that on average stormtime substorms are about twice as intense as, and more than twice as energetic as isolated substorms. The durations of both classes of events were quite identical, about 4 hours. As clear as the differences between isolated and stormtime subtorms are, the question of whether they are produced by the same mechanism is still unclear.

One of the key questions to be answered has been whether the relative importance of the various magnetospheric and ionospheric sinks is a constant for all the events. According to our study, it seems that there are differences in the role of the Joule heating in different types of substorms. The role of the Joule heating decreases when the Sun gets more active. Naturally, the role of the Joule heating is smaller at times of strong ring current activity, i.e. during storms. When analyzing the different types of substorms, it seems evident that the magnetosphere-ionosphere system has several ways

of maintaining the energy input-output balance. Most of the magnetospheric phenomena are controlled by external drivers. However, the structure and dynamics of the magnetosphere also affect the development of magnetic substorms and storms.

Substorms show annual, semiannual and diurnal variations [e.g. *Chapman and Bartels* 1940; *Russell and McPherron,* 1973; *Hamilton and Hodder* 1984]. Our study indicates the semiannual variations in the number, intensity, and Joule dissipation of substorms. The number of substorms was 234 during the spring months (March, April and May), 214 during the fall months, 174 during the summer months (June, July, August) and 217 during the winter months (December (only for December 1997), January and February). It also seems that during equinoxes, the intensities of substorms included in our data set were about 90 nT larger and their typical Joule dissipation was $0.2 \cdot 10^{15}$ J higher than the corresponding values for substorms during solstices. This semiannual variation has been studied in several other papers for over 100 years.

Chapter 5

Discussion of possible sources of errors

Although the main features of heliospheric, magnetospheric and ionospheric phenomena are largely agreed on and the typical parameters characterizing substorms are known, there are several sources of errors in the data analysis. In the estimation of the magnetospheric energy input, the following possible error sources can be identified:

(1) unknown heliospheric and SW-magnetospheric coupling processes;

(2) approximate methods of estimating the energy input;

(3) use of single-point measurements from the upstream solar wind;

(4) measuring solar wind parameters from upstream instead of near magnetopause;

(5) converting ground-based magnetic measurements to the power of Joule heating according to empirical formula;

(6) data resolution;

(7) instrumental errors.

The largest error in the results in our study are most probably caused by the unknown physical processes. The approximate methods of estimating the

energy input cause also uncertainties to the results. One way to improve the estimates of the energy input is to modify the coupling parameter ϵ. One possibility for that is to allow empirical parameter l_0 in the ϵ to be different for different events. Until now, the l_0 has been estimated to be roughly a constant for all the events.

The solar wind homogeneity over spatial scales relevant to solar wind-magnetosphere coupling was studied by comparing the epsilon parameters computed in the upstream solar wind and near the magnetopause. WIND was used as the upstream monitor and IMP 8 was located closer to the magnetopause but still upstream the bow shock. All the 1997 substorms in our data set were analyzed, and in total 13 events were found for which both WIND and IMP 8 solar wind velocity and magnetic field data were available. The WIND data were shifted to the magnetopause (at 10 R_E) and a linear correlation coefficient was computed between W_ϵ from WIND and W_ϵ from IMP 8. The correlation coefficient was as high as 0.96 (figure 5.1), when 60-s data was used. Therefore, upstream solar wind monitors, such as WIND and ACE, can be safely used for magnetospheric energy input computations. This finding is supported by *Coplain et al.* [2001] who found the SOHO and WIND measurements to be consistent with each other. As high correlation as 0.96 makes it evident that data shifting based on the convection time is a good method for shifting of data from the upstream solar wind to the magnetopause. This will be further discussed in a study which is currently under preparation.

The empirical formula 2.20 which converts ground-based magnetic measurements to the power of Joule heating is widely and successfully used. However, it is quite certain that the conversion is not exactly the same for all events. Thus, the conversion is certainly worth of studying in future. Moreover, it needs to be further examined how well the global Joule heating can be approximated to be twice as big as the northern hemisphere Joule dissipation.

Differences caused by the use of low-resolution data (92-s and 60-s) instead of high-resolution data (3-s, 10-s) are studied next. The ϵ parameter was computed from high- and low-resolution data for comparison purposes. The ϵ from the low-resolution data gives 0.5–1.5% difference when compared to the high-resolution data. It is not clear which resolution is more useful for the purposes of this study, because the ionosphere may not react to the changes in the solar wind in time scales of seconds.

Similar errors can be found in respect of the energy dissipation as well. Unknown inner-magnetospheric processes and approximate methods of computing the dissipation causes the largest errors. The use of low-resolution

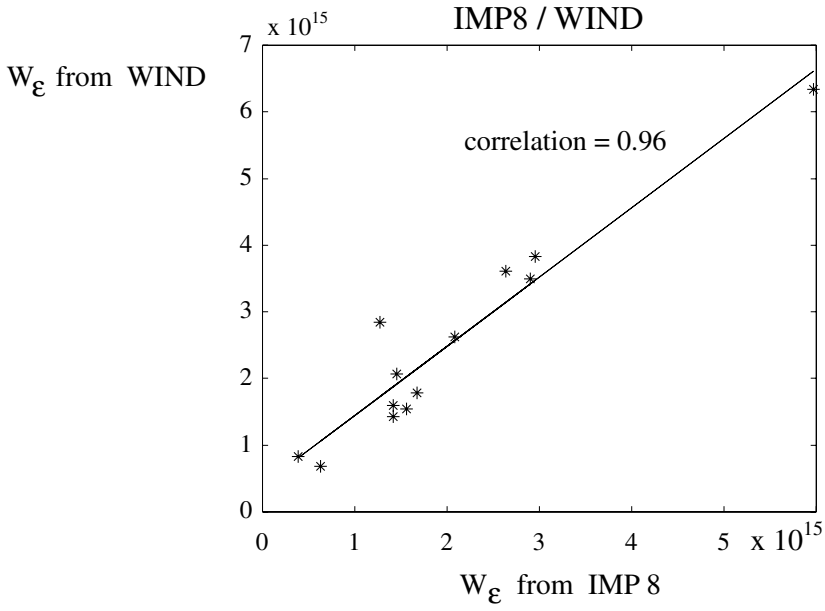

Figure 5.1: Correlation between the W_ϵ from the WIND and the W_ϵ from the IMP 8 when the data in 60-s resolution was used.

IMAGE data instead of high-resolution data as well as instrument errors are insignificant to this study as the natural time scales of the investigated phenomena are of the order of minutes. Furthermore, the integrals are taken over periods of hours.

The limited possibility to measure the phenomena in several places at the same time should also be mentioned. The existing multisatellite campaigns, such as ISTP and Cluster, have made multipoint measurements possible, and thus have improved the possibility to follow the development of magnetospheric dynamics.

Chapter 6

Conclusions

The Sun constantly bursts huge amounts of energy, which is carried via the solar wind into the interplanetary space. Some magnetospheres, such as those of Venus and Mars, have hardly any internal magnetic fields, and thus the solar wind flow gets quite close to the planet. Other planets, such as the Earth, Mercury and Saturn, have strong internal fields, which shield the planets against the bombardment of solar wind particles.

Maintaining the terrestrial magnetosphere consumes about (2–3)$\cdot 10^{12}$ W, which is only a part of the available solar wind kinetic power, (1–2)$\cdot 10^{13}$ W [*Stern,* 1984]. At geomagnetically active times, i.e. during magnetic storms and substorms, there is extra power input from the solar wind into the magnetosphere. The average power dissipated through substorms, estimated by the average epsilon parameter ($< W_\epsilon >$) divided by the average substorm duration, which is about four hours, is about $0.2 \cdot 10^{12}$ W. Thus, the dynamic coupling efficiency during magnetic substorms is about 1%, which is consistent with earlier results [*Stern,* 1984]. Ionospheric dissipation, in particular the Joule heating, covers more than half of the total substorm dissipation, whereas the ring current and plasmoid covers the rest, the plasmoid dissipation being the larger one of those two.

The epsilon parameter [*Akasofu,* 1981] is one of the most widely used coupling functions to estimate the amount of solar wind energy available to the magnetospheric and ionospheric dissipation. This parameter has turned out to be a very useful first-order approximation for the energy input. However, considering the energy carried by plasmoids and the post-plasmoid plasma-sheet flow, and the recent estimates concerning energy dissipation in the inner magnetosphere, rescaling of the epsilon parameter seems to be needed. According to this work, the revision of l_0 from 7 R_E to 9 or 10 R_E

is suggested. This would increase the estimated energy input by a factor of 1.6–2.0.

Substorms occur many times a day, excluding rare longer periods when the substorm activity is modest. Larger storms occur once a month, possibly added by a few of periods with less intense storm activity. Medium-sized storms (*Dst* around –100 nT) consume about 10^{17} J [*Turner et al.,* 2001], whereas typical substorms consume about $2.7 \cdot 10^{15}$ J. However, the yearly total dissipation through substorms seems to be as large as, or even larger than the total dissipation through storms, considering that about 1000-1500 substorms occur each year.

The comparison of isolated and stormtime substorms showed that those two types of events are quite different from each other. The stormtime substorms appeared to be more intense and more energetic than their isolated counterparts. However, due to the much larger amount of isolated events, the total two-year Joule dissipation was considerably larger for isolated substorms ($7.8 \cdot 10^{17}$ J) than for stormtime substorms ($3.4 \cdot 10^{17}$ J). This indicates that the isolated substorms have a more important role in magnetospheric energetics than believed earlier.

6.1 Future

Substorm dynamics is a complex phenomenon which has by no means been exhaustively examined. Substorms are driven by the solar wind, and their energetics are studied by examining magnetic observations measured by the solar wind, high-latitude and low-latitude magnetometers. However, in order to get a complete picture of substorms energetics, the processes in the magnetotail during the substorms need to be studied further. It has also been assumed that the global energy estimates, for example for Joule heating, are twice the northern hemisphere values, which is a question that deserves to be studied more closely in future.

In recent years, plasmoids and other tail processes have increased their role in the substorm energetics. If the present estimates for plasmoid and post–PPS energies can be straightforwardly added to the substorm energy budget, as has been done in the present study, then the role of the tail dissipation is more than one third of the total substorm dissipation. Combined statistical studies on substorm energetics, where the solar wind, ionospheric and tail processes are all studied simultaneously, are still needed. It is known that there are, on average, 1.8 plasmoids during a substorm, but it would be interesting to examine, event by event, what the role of plasmoids in

substorm energetics is.

The magnetosphere shields the Earth rather well from varying solar wind conditions. Still, the substorms near the solar maximum are slightly more frequent and more energetic than the substorms near the solar minimum. It would be useful to study long-term and also seasonal variations in the substorm energetics, particularly during the descending solar cycle phase, when the high speed streams typically exist. Fortunately, there are continuous ground-based and solar wind observations which enable us to examine substorm dynamics in the coming years.

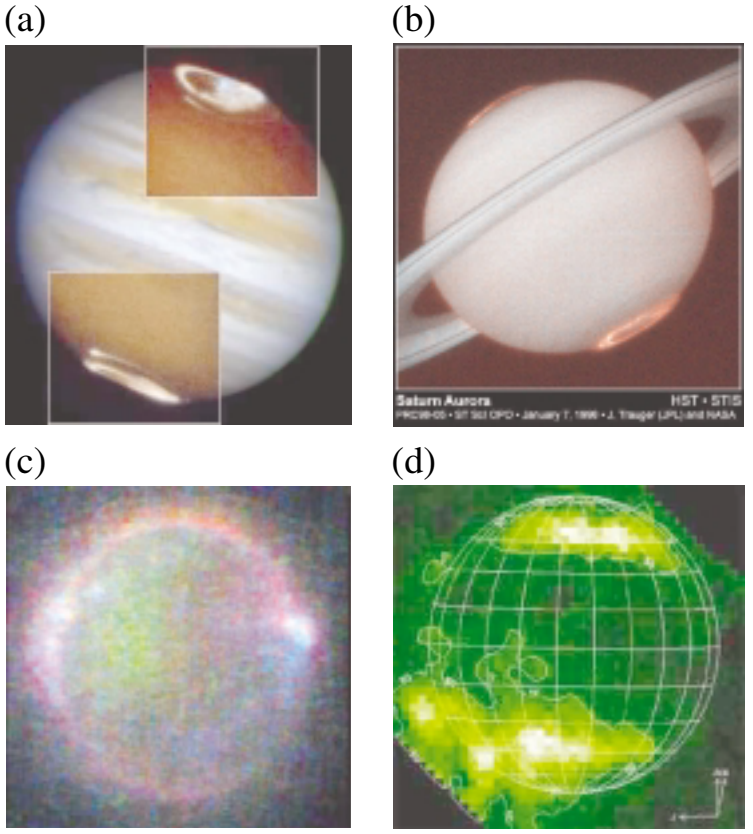

Figure 6.1: Pictures of auroras in ultraviolet light in (a) Jupiter, (b) Saturn, (c) Io and (d) Ganymede. Figures a and b are adapted from http://hubble.stsci.edu/news_.and._views/, figure c from http://galileo.jpl.nasa.gov/images/io/ioeclipse.html and figure d from *Feldman et al.* [2000].

The solar wind interacts with magnetized (e.g. Earth, Mercury) and unmagnetized objects (e.g. Venus, Mars, comets). Even atmosphereless bodies with weak magnetic fields, such as the Moon and asteroids, may cause weak deflections of the solar wind [*Russell,* 2001]. Substorms or substormlike features have been reported to exist on several planets. The Mariner 10 encounter of Mercury brought information on similar variations near Mercury, which are seen in the corresponding regions of the Earth's magnetosphere during substorms [*Siscoe et al.,* 1975]. The Galileo spacecraft near Jupiter observed plasmoids in the jovian tail and explosive reconnection across the current sheet, which both indicate the existence of jovian substorms [*Russell et al.,* 2000]. Auroral emissions, which is an electromagnetic radiation emanating from the high-latitude polar regions, have been observed on several outer planets and their moons [*Bhardwaj and Gladstone,* 2000] (see auroras in figure 6.1.

Studies made on our own magnetosphere contribute to our understanding of the physical processes that may also be operating in other parts of the solar system, and perhaps explain many phenomena in the magnetospheres of other planets, stars and galaxies. And vice versa, observations of other magnetospheres may help us to solve the problems in our own magnetosphere.

6.2 Summary of results

(1) Considering the energy carried by plasmoid and post-plasmoid plasma-sheet flow and the recent estimates of energy dissipation in the inner magnetosphere, rescaling of the epsilon parameter seems to be needed. The revision of l_0 from 7 R_E to 9 or 10 is suggested. This would increase the estimated energy input by a factor of 1.6 – 2.0.

(2) Statistical results from 839 substorms in 1997 and 1999 show that ionospheric dissipation, in particular the Joule heating, covers more than half of the total substorm dissipation. The ring current, plasmoid and post-plasmoid plasma-sheet cover the rest, the tail dissipation being larger than the ring current dissipation.

(3) The size of the substorm, W_{JH}, was found to be determined by the energy input during the substorm expansion phase. Thus, the substorm energetics seems to be largely controlled by the directly driven process. However, loading of energy is needed during the substorm growth phase for the

preconditioning of the magnetosphere.

(4) Internal part of the IL, caused by induction effects, makes 15 to 20% of the IL index during substorm recovery phase, whereas it can be as high as 40% of the IL index during substorm onset. In addition, the internal part of the IL index varies as a function of latitude.

(5) Isolated and stormtime substorms appeared to be quite different from each other. The main differences were that isolated substorms are five times more numerous, but only half as intense as stormtime substorms. However, over a 2-year period two times more energy was dissipated through Joule heating during isolated substorms ($7.8 \cdot 10^{17}$ J) than during stormtime substorms. This indicates that isolated substorms are the main ways of the solar wind energy to be carried to the magnetosphere–ionosphere energy sinks.

(6) Substorms appeared to be more numerous, but only slightly more intense during the high solar activity, in 1999, than during the low solar activity, in 1997. However, the role of Joule heating in the substorm energetics seems to decrease when the Sun becomes more active.

Appendix A

Dst and IL stations

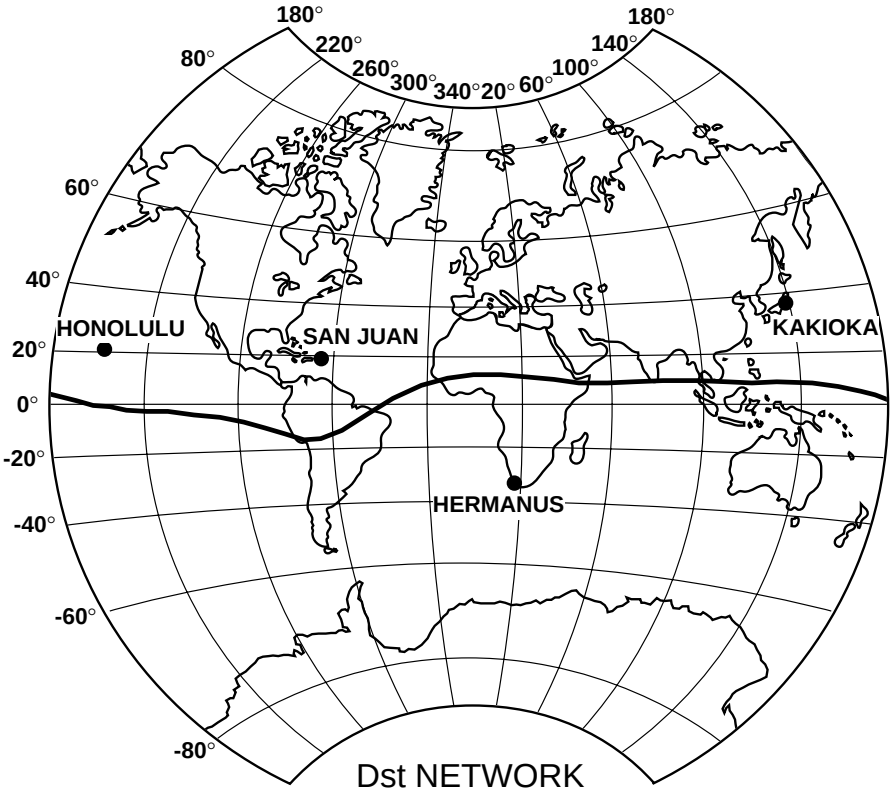

Figure A.1: Four official Dst stations. Adapted from [*Sugiura and Kamei,* 1991].

station		geogr.lat.	geogr.long.	geom.lat.	geom.long.
SJG	San Juan	293.9	18.4	5.2	29.4
HON	Honolulu	202.0	21.3	268.6	21.5
KAK	Kakioka	140.2	36.2	207.8	26.6
HER	Hermanus	19.2	–34.4	82.7	-33.7

Table A.1. *Dst* observatories, their acronyms, geographic and geomagnetic locations.

station		geogr.lat.	geogr.long.	geom.lat.	geom.long.
NAL	Ny Ålesund	78.92	11.95	76.07	112.25
LYR	Longyearbyen	78.20	15.82	75.12	113.00
HOR	Hornsund	77.00	15.60	74.02	110.48
HOP	Hopen Island	76.51	25.01	72.93	115.91
BJN	Bear Island	74.50	19.20	71.33	108.73
SOR	Sørøya	70.54	22.22	67.24	106.71
KEV	Kevo	70.54	27.10	66.21	109.73
TRO	Tromsø	69.76	18.94	66.54	103.44
MAS	Masi	69.46	23.70	66.07	106.92
AND	Andenes	69.30	16.03	66.36	100.92
KIL	Kilpisjärvi	69.02	20.79	65.78	104.31
ABK	Abisko	68.35	18.82	65.21	102.27
MUO	Muonio	68.02	23.53	64.62	105.70
LOZ	Lovozero	67.97	35.08	64.10	114.89
KIR	Kiruna	67.84	20.42	64.60	103.14
SOD	Sodankylä	67.37	26.63	63.82	107.71
PEL	Pello	66.90	24.08	63.46	105.38
LYC	Lycksele	64.61	18.75	61.36	99.73
OUJ	Oulujärvi	64.52	27.23	60.89	106.54
HAN	Hankasalmi	62.30	26.65	58.62	104.99
NUR	Nurmijärvi	60.50	24.65	56.81	102.54
UPS	Uppsala	59.90	17.35	56.45	96.22

Table A.2. IMAGE magnetometer stations, their acronyms, geographic and geomagnetic locations. Vertical lines mark the borders between the different latitudinal zones, which are numbered from south to north (from 1 to 5).

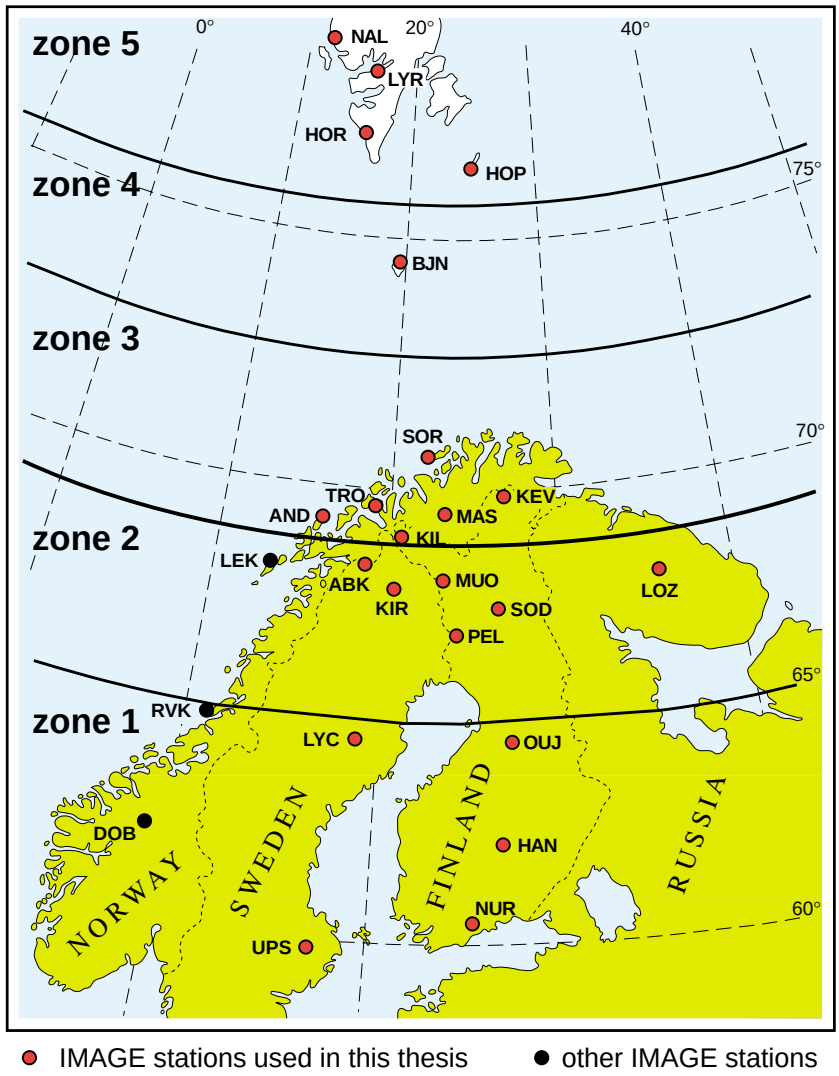

Figure A.2: IMAGE magnetometer stations. The map with magnetometer stations is provided by IMAGE P.I. A. Viljanen and L. Häkkinen.

Appendix B

GSM coordinates

The geocentric solar magnetospheric (GSM) coordinates has its X–axis from the Earth to the Sun. The Y–axis is defined to be perpendicular to the Earth's magnetic dipole, so that the X–Z plane contains the dipole axis. The positive Z–axis is chosen to be in the same sense as the northern magnetic pole.

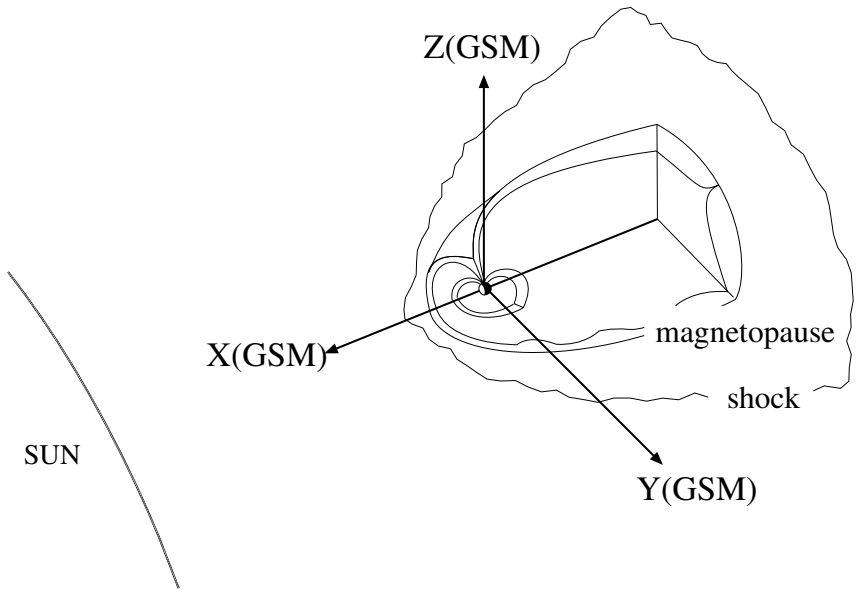

Figure B.1: The geocentric solar magnetospheric (GSM) coordinates.

Appendix C

Acronyms and symbols

C.1 Acronyms

ACE Advanced Composition Explorer spacecraft
AE Auroral electrojet index ($AE = AU - AL$)
AL Index illustrating the strength of the westward auroral electrojets
AMIE Assimilative Magnetosphere Ionosphere Electrodynamics model
AO Measure of the equivalent zonal current ($AO = (AU + AL)/2$)
AU Index illustrating the strength of the eastward auroral electrojets
CANOPUS Longitudinal magnetometer network located over Canada
CME Coronal mass ejection
CL Westward electrojet index which is computed from the CANOPUS measurements
CLUSTER Four-spacecraft mission
CU Eastward electrojet index which is computed from the CANOPUS measurements
DD Directly driven processes
DMI Danish Meteorological Institute
Dst Magnetic stormtime index
Dst* Solar wind pressure corrected Dst index
ep Electron precipitation
EP Substorm Expansion Phase
FMI Finnish Meteorological Institute
GSM Geocentric Solar Magnetospheric coordinates
GP Substorm Growth Phase
IGY International Geophysical Year
IL Westward electrojet index which is computed from the IMAGE measure-

ments
IU Eastward electrojet index which is computed from the IMAGE measurements
IMS International Magnetospheric Study
IMAGE Longitudinal magnetometer chain located into Fennoscandia
IMF Interplanetary magnetic field
IMP 8 Interplanetary Monitoring Platform spacecraft
IS Isolated substorm
ISS International Space Station
ISTP International Solar Terrestrial Program
JH Joule heating
L1 Lagrangian libration point
MAG MAGnetic field experiment in ACE spacecraft
MAGIC Magnetometer chain on the Greenland's ice cap
MFI Magnetic Field Instrument in WIND spacecraft
MI Magnetosphere - Ionosphere -system
MLT Magnetic Local Time
MIRACLE Longitudinal chain located into Fennoscandia, which contains magnetometers, radars and allsky cameras (Magnetometers - Ionospheric Radars - Allsky Cameras Large Experiment)
NENL model Near–Earth Neutral–Line model
PIXIE Polar Ionospheric X-ray Imaging Experiment
POLAR spacecraft
PPS plasmoid plasma-sheet
RC Ring Current - current encircling the Earth at the equatorial plane
RP Substorm Recovery Phase
SI International System (of units of measurements)
SMI Solar wind - Magnetosphere - Ionosphere -system
$\mathbf{S_{cont}}$ Substorms where there was energy input during the entire substorm period
$\mathbf{S_{equ}}$ Substorms occurring south from the standard AE magnetometer station Abisko
$\mathbf{S_{pole}}$ Substorms occurring north from the standard AE magnetometer station Abisko
$\mathbf{S_{GP}}$ Substorms where there was energy input mainly during the substorm growth phase
SS Stormtime substorm
S97 Substorm occurring during the year low solar activity, in 1997)
S99 Substorm occurring during the year of high solar activity, in 1999
SOHO Spacecraft in solar wind

SW Solar wind
SWE Solar Wind Experiment in WIND spacecraft
SWEPAM Solar Wind Electron Proton Alpha Monitor in ACE spacecraft
TCR Traveling Compression Region
UT Universal Time
UVI UltraViolet Imager
WIND NASA spacecraft

C.2 Symbols

A Surface area of the tail magnetopause
A_{JH} xy-plane in GSM coordinates, where the Joule heating collisions occur
B Magnetic field
B_0 magnetic field intensity at the equator
B_n normal magnetic field component
B_s southward component of the total magnetic field
B_t tangential magnetic field component
B_x IMF X-component in GSM coordinate system
B_y IMF Y-component in GSM coordinate system
B_z IMF Z-component in GSM coordinate system
B_T transverse magnetic field
E electric field
f frequency of substorms
I substorm intensity
j current density
J height-integrated current
l_0 empirical parameter to fit the energy input to the total estimated output
L_x plasmoid length
L_y plasmoid width
L_z plasmoid height
n number of substorms
p solar wind dynamic pressure
P power of magnetospheric dynamo
P_{ep} electron precipitation power
P_{JH} Joule heating power
P_S substorm power
Q_{JH} Joule heating rate
R_{CF} Chapman–Ferraro radius

R_E Earth radii
S poynting flux
t time
T total time when substorms occurred
t_b start time of the substorm
t_e end time of substorm
t_o substorm onset
v velocity
V_{JH} Volume in GSM coordinates where the Joule heating occurs.
W_ϵ energy input
W_{ep} electron precipitation energy
$W_{ionosphere}$ ionospheric dissipation
W_{ip} ion precipitation energy
W_{IN} total magnetospheric energy input
W_{JH} Joule heating energy
W_{OUT} total magnetospheric energy output
W_{RC} ring current energy
X IMF x-component in GSM coordinate system
X_{ext} external part of X-component
X_{int} internal part of X-component
Y IMF y-component in GSM coordinate system
Z IMF z-component in GSM coordinate system
Δt substorm duration
ΔH north-south component of the magnetic disturbance
ΔX distance between the data-producing spacecraft and the nose of the magnetopause
ϵ epsilon parameter, which is a magnetosphere ionosphere coupling function
ϵ_T transverse epsilon parameter
ϵ^* ram-pressure corrected epsilon parameter
θ IMF clock angle in GSM coordinates
μ_0 permeability of free space
ρ solar wind density
σ_P Pedersen conductivity
Σ_H height-integrated Hall conductivity
Σ_P height-integrated Pedersen conductivity
τ ring current decay time

Bibliography

Ahn, B.-H., S.-I. Akasofu, and Kamide Y., The Joule heat production rate and the particle energy injection rate as a function of the geomagnetic indices AE and AL, *J. Geophys. Res., 88*, 6275, 1983.

Akasofu, S.-I., The development of the auroral substorm, *Planet Space Sci., 12*, 273, 1964.

Akasofu, S.-I., S. Chapman, and C.-I. Meng, The polar electrojet, *J. Atmos. Terr. Phys., 27*, 1275, 1965.

Akasofu, S.-I., Polar and Magnetospheric substorms, *Astrophysics and Space Science library, vol. 11* edited by S.-I. Akasofu, D. Reidel Pub. Co, Dordrecht, Holland, 1968.

Akasofu, S.-I., Interplanetary energy flux associated with magnetospheric substorms, *Planet Space Sci., 27*, 425, 1979.

Akasofu, S.-I., The solar wind-magnetosphere energy coupling and magnetosphere disturbances, *Planet Space Sci., 28*, 495, 1980.

Akasofu, S.-I., Energy coupling between the solar wind and the magnetosphere, *Space Sci. Rev., 28*, 121, 1981.

Akasofu, S.-I., and Chapman, S., The ring current, geomagnetic disturbance, and Van Allen radiation belts, *J. Geophys. Res., 66*, 1321, 1961.

Baker, D. N.,E.W. Jr. Hones, P.R. Higbie, R.D. Belian, P. Stauning, Global properties of the magnetosphere during a substorm growth phase: A case study, *J. Geophys. Res., 86*, 8941, 1981.

Baker, D. N., S.-I. Akasofu, W. Baumjohann, J.W. Bieber, D. H. Fairfield, E. W. Hones Jr., B. Mauk, R. L. McPherron, and T. E. Moore, Substorms in the magnetosphere, in *Solar Terrestrial Physics - Present and Future, NASA Publ., 1120*, 1984.

Baker, D. N.,T. I. Pulkkinen, V. Angelopoulos, W. Baumjohann, and R. L. McPherron, The neutral line model of substorms: Past results and present view, *J. Geophys. Res., 101*, 12, 975, 1996.

Bargatze, L. F., D. N. Baker, R. L. McPherron, and E. W. Hones, Jr., Magnetospheric impulse response for many levels of geomagnetic activity, *J. Geophys. Res., 90*, 6387, 1985.

Bargatze, L. F., R.L. McPherron, and D.N. Baker, Solar wind-magnetosphere energy input function, in: *Solar Wind-Magnetosphere Coupling, Geophys. Monogr. Ser.*, vol. 126, edited by Y. Kamide and J.A. Slavin, p. 101, AGU, Washington, D.C., 1986.

Baumjohann, W., and Y. Kamide, Hemispherical Joule Heating and the AE Indices, *J. Geophys. Res., 89*, 383, 1984.

Baumjohann, W., Some recent progress in substorm studies, *J. Geomagn. Geoelectr., 38*, 633, 1986.

Baumjohann, W., Y. Kamide, and R. Nakamura, Substorms, storms, and the near-Earth tail, *J. Geomagn. Geoelectr., 48*, 177, 1996.

Bhardwaj, A. and G. R. Gladstone, Auroras on Saturn, Uranus, and Neptune, *Adv. Space Res., 26*, 1551, 2000.

Birkeland, K., *The Norwegian Aurora Polaris Expedition 1902-1903*, vol.1, 1st sect., Aschhoug, Oslo, Norway, 1908.

Borovsky J.E., R.J. Nemzek, and R. D. Belian, The occurrence rate of magnetospheric substorm onsets - Random and periodic substorms, *J. Geophys. Res., 98*, 3807, 1993.

Boström, R.A., A model of the auroral electrojets, *J. Geophys. Res., 69*, 4983, 1964.

Burton, R.K., R.L. McPherron, and C.T. Russell, An empirical relationship between interplanetary conditions and *Dst*, *J. Geophys. Res., 80*, 4204, 1975.

Caan, M.N., R.L. McPherron, and C.T. Russell, The statistical magnetic signature of magnetospheric substorms, *Planet Space Sci., 26*, 269, 1978.

Chapman, S., and Bartels, J., *Geomagnetism*, Vol 1. Oxford University Press, New York (Chapter 11), 1940.

Chapman, S., and V.C.A. Ferraro, A new theory of magnetic storms, Part I - The initial phase, *Terrestrial Magnetism and Atmospheric Electricity, 36*, 171, 1931.

Chapman, S., and V.C.A. Ferraro, A new theory of magnetic storms, Part I - The initial phase continued, *Terrestrial Magnetism and Atmospheric Electricity, 37*, 421, 1932.

Chapman, S., and V.C.A. Ferraro, A new theory of magnetic storms, Part II - The main phase, *Terrestrial Magnetism and Atmospheric Electricity, 38*, 79, 1933.

Chree, C., *Encyclopaedia Britannica, 11th ed.*, vol 17, pp.353, 1911.

Chree, C., *Studies in Terrestrial magnetism*, pp.206, McMillan and Co., London and New York, 1912.

Clauer, C.R., R.L. McPherron, C. Searls, and M.G. Kivelson, Solar wind control of auroral zone geomagnetic activity, *Geophys. Res. Lett., 8*, 915, 1981.

Coplain, M.A., F. Ipavich, J. King, K.W. Ogilvie, D.A. Roberts, and A.J. Lazarus, Correlation of solar wind parameters between SOHO and Wind, *J. Geophys. Res., 106*, 18615, 2001.

Davis, T.N., and M. Sugiura, Auroral electrojet activity index AE and its universal time variations, *J. Geophys. Res., 71*, 785, 1966.

Dungey, J.W., Conditions for the occurrence of electrical discharge in astrophysical systems, *Philos. Mag., 44*, 725, 1953.

Dungey, J.W., Interplanetary magnetic field and the auroral zones, *Phys. Rev. Lett., 6*, 47, 1961

Fairfield, D.H, and L.J. Jr. Cahill., Transition region magnetic field and polar magnetic disturbances, *J. Geophys. Res., 71*, 155, 1966.

Feldman, P.D., M.A. McGrath, D.F. Strobel, H.W. Moos, K.D. Rutherford, and B.C. Wolves, HST/STIS Ultraviolet imaging of polar aurora on ganymede, *Astrophys. J., 353*, 1085, 2000.

Giovanelli, R.G., Magnetic and electric phenomena in the Sun's atmosphere associated with sunspots, *Month.Not.Roy.Astr.Soc., 107*, 338, 1947.

Gold, T., Motions in the magnetosphere of the Earth, *J. Geophys. Res., 64*, 1219, 1959a.

Gold, T., Plasma and magnetic fields in the solar system, *J. Geophys. Res., 64*, 1665, 1959b.

Gonzalez, W.D., and B.T. Tsurutani, Criteria of interplanetary parameters causing intense magnetic storms (Dst < –100 nT) , *Planet. Space Sci., 35*, 1101, 1987.

Hamilton, D.C., and B.M. Hodder, The influence of sunspot number and magnetic activity on the diurnal variation of the geomagnetic field at mid to high latitudes, *J. Atmos. Terr. Phys., 46*, 193, 1984.

Hamilton, D.C., G. Gloeckler, F.M. Ipavich, W. Studemann, B. Wilken, and G. Kremser, Ring current development during the great geomagnetic storm on February, 1986, *J. Geophys. Res., 943*, 14343, 1988.

Hardy D.A., M.S. Gussenhoven, and D. Brautigam, *J. Geophys. Res., 94*, 370, 1989.

Häkkinen, L.V.T., T.I. Pulkkinen, R. Pirjola, H. Nevanlinna, E.I. Tanskanen, and N.E. Turner, Seasonal and diurnal variation of geomagnetic activity: revised Dst vs. external drivers, *J. Geophys. Res., submitted*, 2002b.

Häkkinen, L.V.T., T.I. Pulkkinen, H. Nevanlinna, R. Pirjola, and E.I. Tanskanen, Effects of induced currents on Dst and on magnetic variations at mid-latitude stations, *J. Geophys. Res., in press*, 2002a.

Hones, E.W., Jr., The magnetotail: Its generation and dissipation, in *Physics of Solar Planetary Environments, Proceedings of the International Symposium on Solar-Terrestrial Physics*, edited by D.J. Williams, p. 558, AGU, Washington, D.C., 1976

Hones, E.W., Jr., T. Pytte, and H.I. West Jr., Association of geomagnetic activity with plasma sheet thinning and expansion: A statistical study, *J. Geophys. Res., 89*, 5471, 1984.

Hsu, T.-S., and R.L. McPherron, The characteristics of storm-time substorms and non-storm substorms, Proceedings of the International Conference on Substorms (ICS-5), ESA SP-443, p.439, 2000.

Hughes, W.J., and D.G. Sibeck, On the 3-dimensional structure of plasmoids, *Geophys. Res. Lett., 14*, 636, 1987.

Ieda, A., S. Machida, T. Mukai, Y. Saito, T. Yamamoto, A. Nishida, T. Terasawa, and S. Kokobun, Statistical analysis on the plasmoid evolution with Geotail observations, *J. Geophys. Res., 103*, 4453, 1998.

Kamide, Y., The two-component auroral electrojet , *Geophys. Res. Lett., 9*, 10, 1175, 1982.

Kamide, Y., and A.D. Richmond, Ionospheric conductivity dependence of electric fields and currents estimated from ground magnetic observations, *J. Geophys. Res., 87*, 8331, 1982.

Kamide, Y., and W. Baumjohann, *Magnetosphere-ionosphere Coupling*, Springer-Verlag, New York, 1993.

Kamide, Y., W. Baumjohann, I.A. Daglis, W.D. Gonzales, M. Grande, J.A. Joselyn, R.L. McPherron, J.L. Phillips, G.D. Reeves, G. Rostoker, A.S. Sharma, H.J. Singer, B.T. Tsurutani, and V.M. Vasyliunas, Current understanding of magnetic storms: storm-substorm relationship, *J. Geophys. Res., 103*, 17705, 1998.

Kan, J. R., L.C. Lee, and S.-I. Akasofu, The energy coupling function and the power generated by the solar wind-magnetosphere dynamo, *Planet Space Sci., 28*, 823, 1980.

Kan, J. R., and S.-I. Akasofu, Dynamo process governing solar wind-magnetosphere energy coupling, *Planet Space Sci., 30*, 367, 1982.

Kauristie, K., T. I. Pulkkinen, R.J. Pellinen, and H. J. Opgenoorth, What can we tell about auroral electrojet activity from a single meridional magnetometer chain, *Ann. Geophys., 14*, 1177-1185, 1996.

Knipp D.J., B.A. Emery, M. Engebretson, X. Li, A.H. McAllister, T. Mukai, S. Kokobun, G.D. Reeves, D. Evans, T. Obara, X. Pi, T. Rosenberg, A. Weatherwax, M.G. McHarg, F.Chun, K. Mosely, M. Codescu, L. Lanzerotti, F.J. Rich, J. Sharber, and P. Wilkinson, An overview of the early November 1993 geomagnetic storm, *J. Geophys. Res., 103*, 26197, 1998.

Le, G., C.T. Russell, J.T. Gosling, M.F. Thomsen, ISEE observations of low-latitude boundary layer for northward interplanetary magnetic field: implications for cusp reconnection *J. Geophys. Res., 101*, 27239, 1996.

Lepping, R.P., M.H. Acuna, L.F. Burlaga, W.M. Farrel, J.A. Slavin, K.H. Schatten, F. Mariani, N.F. Ness, F.M. Neubauer, Y.C. Whang, J.B. Byrnes, R.S. Kennon, P.V. Panetta, J. Scheifele, and E.M. Worley, The Wind magnetic field investigation, *Space Sci. Rev., 71*, 207–229, 1995.

Lu, G., D. N. Baker, R. L. McPherron, C. J. Farrugia, D. Lummerzheim, J. M. Ruohoniemi, F. J. Rich, D. S. Evans, R. P. Lepping, M. Brittnacher, X. Li, R. Greenwald, G. Sofko, J. Villain, M. Lester, J. Thayer, T. Moretto, D. Milling, O. Troshichev, A. Zaitzev, V. Odintzov, G. Makarov, and K. Hayashi, Global energy deposition during the January 1997 magnetic cloud event, *J. Geophys. Res., 103*, 11685, 1998.

Lui, A.T.Y., R.E. Lopez, S.M. Krimigis, R.W. McEntire, L.J. Zanetti, and T.A. Potemra, A case study of magnetotail current sheet disruption and diversion, *Geophys. Res. Lett., 15(7)*, 721, 1988.

Mac-Mahon R.M., and W.D. Gonzalez, Energetics during the main phase of geomagnetic superstorms, *J. Geophys. Res.,102*, 14199, 1997.

Mayaud, P.N., Deviation, Meaning, and Use of Geomagnetic Indices, *AGU Geophysical Monographs, New perspectives on the Earth's magnetotail, 22*, 1980.

McComas, D.J., S.J. Bame, P. Barker, W.C. Feldman, J.L. Phillips, P. Riley, and J.W. Griffee, Solar wind electron proton alpha monitor (SWEPAM) for the advanced composition explorer, *Space Sci. Rev., 86*, 563, 1998.

McPherron, R.L., Relation of auroral zone micropulsations to magnetospheric substorms, *Thesis(PH.D.), Vol. 29-12. section B*, page 4780, 1968.

McPherron, R.L., Growth phase of magnetospheric substorms, *J. Geophys. Res.,75*, 5592, 1970.

McPherron, R.L., Magnetospheric substorms, *Rev. Geophys. Space Phys., 17*, 657, 1979.

McPherron R.L., Physical processes producing magnetospheric substorms and magnetic storms, in *Geomagnetism*, vol 4, edited by J. Jacobs, pp. 593, Academic, San Diego, Calif., 1991.

McPherron, R.L., C.T. Russell, and M.P. Aubry, Satellite studies of magnetospheric substorms on August 15, 1968, 9. Phenomenological Model for substorms, *J. Geophys. Res., 78*, 3131, 1973.

O'Brien, T.P., and R.L. McPherron, An empirical phase space analysis of ring current dynamics: Solar wind control of injection and decay, *J. Geophys. Res.,105*, 7707, 2000.

Ogilvie K.W., D.J. Chornay, R.J. Fritzenreiter, F. Onsaker, J. Keller, J. Lobell, G. Miller, J.D. Scudder, and E.C. Sittler, JR., SWE, A Comprehensive plasma instrument for the WIND spacecraft, *Space Sci. Rev., 71*, 55–77, 1995.

Østgaard, N., R.R. Vondrak, J.W. Gjerloev, and G.A. Germany, A relation between the energy deposition by electron precipitation and geomagnetic indices during substorms, *J. Geophys. Res.,*–, –, 2002, in press.

Paschmann, G., B.U.O. Sonnerup, I. Papamastorakis, N. Sckopke, G. Haerendel, S.J. Blame, J.R. Asbridge, J.T. Gosling, C.T. Russell, and R.C. Elphic, Plasma acceleration at the earth's magnetopause: Evidence for reconnection, *Nature*, 282, 1979.

Perreault, P., and S.-I. Akasofu, A study of geomagnetic storms, *Geophys. J. R. Astr. Soc., 54*, 547, 1978.

Pulkkinen, T.I., N. Yu. Ganushkina, E.I. Kallio, G. Lu, D.N. Baker, N.E. Turner, T.A. Fritz, J.F. Fennell, J. Roeder, Energy dissipation during a geomagnetic storm: May 1998, *Adv. Space Res., in press*, 2002.

Rangarajan, G.K., Indices of Geomagnetic Activity, in *Geomagnetism*, vol 3, edited by J.A. Jacobs, p. 323, Academic Press, London, 1989.

Rostoker, G., S.-I. Akasofu, J. Foster, R.A. Greenwald, Y. Kamide, K. Kawasaki, A.T.Y. Lui, R.L McPherron, and C.T. Russell, Magnetospheric Substorms - Definition and Signatures, *J. Geophys. Res., 85*, 1663, 1980.

Rostoker, G., J.C. Samson, F. Creutzberg, T.J. Hughes, D.R. McDiarmid, A.G. McNamara, A. Vallance Jones, D.D. Wallis, and L.L. Cogger, CANOPUS: A groundbased instrument array for remote sensing the high latitude ionosphere during the ISTP/GGS program, *Space Sci. Rev., 71*, 743, 1995.

Russell, C.T., The dynamics of planetary magnetospheres, *Planet. Space Sci., 49*, 1005, 2001

Russell, C.T., and R.L. McPherron, Semiannual variation of geomagnetic activity, *J. Geophys. Res., 78*, 92, 1973.

Russell, C.T., K.K. Khurana, M.G. Kivelson, and D.E. Huddleston, Substorms at Jupiter: Galileo observations of transient reconnection in the near tail, *Adv. Space Sci.., 26*, 1499, 2000.

Scholer, M., G. Gloeckler, D. Hovestadt, B. Klecker, F.M. Ipavich, Characteristics of the plasmoidlike structures in the distant magnetotail, *J. Geophys. Res., 89*, 8872, 1984b.

Scholer, M., G. Gloeckler, B. Klecker, F.M. Ipavich, D. Hovestadt, E.J. Smith, Fast moving plasma structures in the distant magnetotail, *J. Geophys. Res., 89*, 6717, 1984a.

Shue, J.H., J.K. Chao, H.C. Fu, C.T. Russell, P. Song, K.K. Khurana, and H.J. Singer, A new functional form to the study the solar wind control of the magnetopause size and shape, *J. Geophys. Res., 102*, 9497, 1997.

Shue, J.H., P. Song, C.T. Russell, J.T. Steinberg, J.K. Chao, G. Zastenker, O.L. Vaisberg, S. Kokobun, H.J. Singer, T.R. Detman, and H. Kawano, Magnetopause location under extreme solar wind conditions, *J. Geophys. Res., 103*, 17691, 1998.

Siscoe, G.L., Evidence in the auroral record for secular solar variability, *Reviews of Geophysical and Space Physics, 18*, 647, 1980.

Siscoe, G.L., N.F. Ness, and C.M. Yeates, Substorms in Mercury? *J. Geophys. Res., 80*, 4359, 1975.

Slavin J.A., E.J. Smith, B.T. Tsurutani, D.G. Sibeck, H.J Singer, D.N. Baker, J.T. Gosling, E.W. Hones, and F.L. Scarf, Substorm accociated traveling compression regions in the distant tail - ISEE-3 geotail observations, *Geophys. Rev. Lett., 11*, 657, 1984.

Slavin J.A., M.F. Smith, E.L. Mazur, D.N. Baker, T. Iyemori, and E.W. Greenstadt, ISEE 3 observations of traveling compression regions in the Earth's magnetotail, *J. Geophys. Res., 98*, 15425, 1993.

Slavin J.A., Traveling compression regions, *AGU Geophysical Monographs, New perspectives on the Earth's magnetotail, 105*, 1998.

Smith, C.W., J. L'Heureux, N.F. Ness, M.H. Acuna, L.F. Burlaga, and J. Scheifele, The ACE magnetic fields experiments, *Space Sci. Rev., 86*, 613, 1998.

Song Y., and R.L. Lysak, Current dynamo effects of 3-D time-dependent reconnection in the dayside magnetopause *Geophys. Res. Lett., 16*, 911, 1989.

Spiro R.W., P.H. Reiff, and L.J. Maher, Jr., Precipitating electron energy flux and auroral zone conductances - an empirical model, *J. Geophys. Res., 87*, 8215, 1982.

Stern D.P., Energetics of the magnetosphere, *Space Sci. Rev., 39*, 193, 1984.

Stauning, P., C.R. Clauer, T.J. Rosenberg, E. Friis-Christensen, and R. Sitar, Observations of solar-wind-driven progression of interplanetary magnetic field BY-related ionospheric disturbances, *J. Geophys. Res., 100*, 7567, 1995.

Sugiura, M., Hourly values of equatorial *Dst* for the IGY *Ann. Int. Geophys. Year, 35*, 49, 1964.

Sugiura, M., and S. Hendricks, Provisional hourly values of equatorial Dst for 1961, 1962 and 1963, NASA *Tech. note D-4047*, 1967.

Sugiura, M., and T. Kamei, Equatorial Dst index 1957–1986, in *IAGA Bulletin 40*, edited by A. Berthelier, and M. Menvielle, ISGI Publ. Off. Saint Maur, 1991.

Syrjäsuo, M., T. I. Pulkkinen, R. J. Pellinen, P. Janhunen, K. Kauristie, A. Viljanen, H. J. Opgenoorth, P. Karlsson, S. Wallman, P. Eglitis, O. Amm, E. Nielsen, and C. Thomas, Observations of substorm electrodynamics using the MIRACLE network, in: *Substorms-4*, edited by S. Kokubun and Y. Kamide, Terra Scientific Publishing Company, Tokyo, pp. 111–114, 1998.

Turner, N.E., D.N. Baker, T.I. Pulkkinen, G. Lu, Global energy partitioning during magnetic storms, *J. Geophys. Res., submitted*, 2001.

Vasyliunas, V.M., Joseph R. Kan, George L. Siscoe and S.-I. Akasofu, Scaling relations governing magnetospheric energy transfer, *Planet Space Sci., 30*, 359, 1982.

Viljanen, A., K. Kauristie, and K. Pajunpää, On induction effects at EISCAT and IMAGE magnetometer stations, *Geophys. J. Int, 121*, 893, 1995.

Weaver, J.T., On the separation of local geomagnetic fields into external and internal parts, *Z. Geophys., 30*, 29, 1964.

Weiss L.A., P.H. Reiff, J.J. Moses, R.A. Heelis, and B.D. Moore, Energy dissipation in substorms, Proceedings of the International Conference on Substorms (ICS-1), ESA SP-335, pp.309-317, 1992.

Zwickl, R.D., et al., An evaluation of the total magnetospheric energy output parameter, U_T, in *Magnetotail Physics*, A.T.Y. Lui, Editor, Johns Hopkins University Press, Baltimore, p. 155, 1987.